Systematic studies of correlations between different order flow harmonics in Pb-Pb collisions at $\sqrt{s_{NN}} = 2.76$ TeV

S. Acharya *et al.*[*]
(ALICE Collaboration)

(Received 1 October 2017; published 12 February 2018)

The correlations between event-by-event fluctuations of anisotropic flow harmonic amplitudes have been measured in Pb-Pb collisions at $\sqrt{s_{NN}} = 2.76$ TeV with the ALICE detector at the Large Hadron Collider. The results are reported in terms of multiparticle correlation observables dubbed symmetric cumulants. These observables are robust against biases originating from nonflow effects. The centrality dependence of correlations between the higher order harmonics (the quadrangular v_4 and pentagonal v_5 flow) and the lower order harmonics (the elliptic v_2 and triangular v_3 flow) is presented. The transverse momentum dependences of correlations between v_3 and v_2 and between v_4 and v_2 are also reported. The results are compared to calculations from viscous hydrodynamics and a multiphase transport (AMPT) model calculations. The comparisons to viscous hydrodynamic models demonstrate that the different order harmonic correlations respond differently to the initial conditions and the temperature dependence of the ratio of shear viscosity to entropy density (η/s). A small average value of η/s is favored independent of the specific choice of initial conditions in the models. The calculations with the AMPT initial conditions yield results closest to the measurements. Correlations among the magnitudes of v_2, v_3, and v_4 show moderate p_{T} dependence in midcentral collisions. This might be an indication of possible viscous corrections to the equilibrium distribution at hadronic freeze-out, which might help to understand the possible contribution of bulk viscosity in the hadronic phase of the system. Together with existing measurements of individual flow harmonics, the presented results provide further constraints on the initial conditions and the transport properties of the system produced in heavy-ion collisions.

DOI: 10.1103/PhysRevC.97.024906

I. INTRODUCTION

The main emphasis of the ultrarelativistic heavy-ion collision programs at the Relativistic Heavy Ion Collider (RHIC) and the Large Hadron Collider (LHC) is to study the deconfined phase of strongly interacting QCD matter, the quark-gluon plasma (QGP). The matter produced in a heavy-ion collision exhibits strong collective radial expansion [1,2]. Difference in pressure gradients and the interactions among matter constituents produced in the spatially anisotropic overlap region of the two colliding nuclei result in anisotropic transverse flow in the momentum space. The large elliptic flow discovered at RHIC energies [3–7] is also observed at LHC energies [8–18]. The measurements are well described by calculations utilizing viscous hydrodynamics [19–24]. These calculations also demonstrated that the shear viscosity to the entropy density ratio (η/s) of the QGP in heavy-ion collisions at RHIC and LHC energies is close to a universal lower bound $1/4\pi$ [25].

The temperature dependence of η/s has some generic features typical to the most known fluids. This ratio reaches its minimum value close to the phase transition region [25,26]. It was shown, using kinetic theory and quantum mechanical considerations [27], that $\eta/s \sim 0.1$ would be the correct order of magnitude for the lowest possible shear viscosity to entropy density ratio value found in nature. Later it was demonstrated that an exact lower bound $(\eta/s)_{\mathrm{min}} = 1/4\pi \approx 0.08$ can be conjectured using anti-de sitter/conformal field theory (AdS/CFT) correspondence [25]. Hydrodynamical simulations constrained by data support the view that η/s of the QGP is close to that limit [23]. It is argued that such a low value might imply that thermodynamic trajectories for the expanding matter would lie close to the quantum chromodynamics (QCD) critical end point, which is another subject of intensive experimental study [26,28].

Anisotropic flow [29] is quantified with nth-order flow harmonics v_n and corresponding symmetry plane angles Ψ_n in a Fourier decomposition of the particle azimuthal distribution in the plane transverse to the beam direction [30,31]:

$$E\frac{d^3N}{d^3p} = \frac{1}{2\pi}\frac{d^2N}{p_{\mathrm{T}}dp_{\mathrm{T}}d\eta} \times \left\{1 + 2\sum_{n=1}^{\infty} v_n(p_{\mathrm{T}},\eta)\cos[n(\varphi - \Psi_n)]\right\}, \quad (1)$$

where E, p, p_{T}, φ, and η are the particle's energy, momentum, transverse momentum, azimuthal angle, and pseudorapidity, respectively, and Ψ_n is the azimuthal angle of the symmetry

[*]Full author list given at the end of the article.

plane of the nth-order harmonic. Harmonic v_n can be calculated as $v_n = \langle \cos[n(\varphi - \Psi_n)] \rangle$, where the angular brackets denote an average over all particles in all events. The anisotropic flow in heavy-ion collisions is typically understood as the hydrodynamic response of the produced matter to spatial deformations of the initial energy density profile [32]. This profile fluctuates event by event due to fluctuating positions of the constituents inside the colliding nuclei, which implies that v_n also fluctuates [33,34]. The recognition of the importance of flow fluctuations led to the discovery of triangular and higher flow harmonics [9,35] as well as to the correlations between different v_n harmonics [36,37]. The higher order harmonics are expected to be sensitive to fluctuations in the initial conditions and to the magnitude of η/s [38,39], while v_n correlations have the potential to discriminate between these two respective contributions [36].

Difficulties in extracting η/s in heavy-ion collisions can be attributed mostly to the fact that it strongly depends on the specific choice of the initial conditions in the models used for comparison [19,39,40]. Viscous effects reduce the magnitude of the anisotropic flow. Furthermore, the magnitude of η/s used in hydrodynamic calculations should be considered as an average over the temperature evolution of the expanding fireball as it is known that η/s depends on temperature. In addition, part of the anisotropic flow can also originate from the hadronic phase [41–43]. Therefore, both the temperature dependence of η/s and the relative contributions from the partonic and hadronic phases should be understood better to quantify the η/s of the QGP.

An important input to the hydrodynamic model simulations is the initial distribution of energy density in the transverse plane (the initial density profile), which is usually estimated from the probability distribution of nucleons in the incoming nuclei. This initial energy density profile can be quantified by calculating the distribution of the spatial eccentricities ϵ_n [35],

$$\varepsilon_n e^{in\Phi_n} = -\{r^n e^{in\phi}\}/\{r^n\}, \tag{2}$$

where the curly brackets denote the average over the transverse plane, i.e., $\{\cdots\} = \int dxdy\, e(x,y,\tau_0)\,(\cdots)$, r is the distance to the system's center of mass, ϕ is azimuthal angle, $e(x,y,\tau_0)$ is the energy density at the initial time τ_0, and Φ_n is the participant plane angle (see Refs. [44,45]). There is experimental and theoretical evidence [9,35,46] that the lower order harmonics, v_2 and v_3, to a good approximation, are linearly proportional to the deformations in the initial energy density in the transverse plane (e.g., $v_n \propto \varepsilon_n$ for $n = 2$ or 3). Higher order ($n > 3$) flow harmonics can arise from initial anisotropies in the same harmonic [35,44,47,48] (linear response) or can be induced by lower order harmonics [49,50] (nonlinear response). For instance, v_4 can develop both as a linear response to ε_4 and/or as a nonlinear response to ε_2^2 [51]. Therefore, the higher harmonics ($n > 3$) can be understood as superpositions of linear and nonlinear responses, through which they are correlated with lower order harmonics [47,48,50,52,53]. When the order of the harmonic is large, the nonlinear response contribution in viscous hydrodynamics is dominant and increases in more peripheral collisions [50,52]. The magnitudes of the viscous corrections as a function of p_{T} for v_4 and v_5 are sensitive to the ansatz used for the viscous distribution function, a correction for the equilibrium distribution at hadronic freeze-out [52,54]. Hence, studies of the correlations between higher order ($n > 3$) and lower order (v_2 or v_3) harmonics and their p_{T} dependence can help to understand the viscous correction to the momentum distribution at hadronic freeze-out which is among the least understood parts of hydrodynamic calculations [45,52,55,56].

The first results for new multiparticle observables which quantify the relationship between event-by-event fluctuations of two different flow harmonics, the *symmetric cumulants* (SC), were recently reported by the ALICE Collaboration [57]. The new observables are particularly robust against few-particle nonflow correlations [8] and they provide independent, complementary information to recently analyzed symmetry plane correlators [37]. It was demonstrated that they are sensitive to the temperature dependence of η/s of the expanding medium and therefore simultaneous descriptions of correlations between different order harmonics would constrain both the initial conditions and the medium properties [57,58]. In this article, we have extended the analysis of SC observables to higher order harmonics (up to fifth order) as well as to the measurement of the p_{T} dependence of correlations for the lower order harmonics (v_3-v_2 and v_4-v_2). We also present a systematic comparison to hydrodynamic and AMPT model calculations. In Sec. II we present the analysis methods and summarize our findings from the previous work [57]. The experimental setup and measurements are described in Sec. III. The sources of systematic uncertainties are explained in Sec. IV. The results of the measurements are presented in Sec. V. In Sec. VI we present comparisons to model calculations. Finally, Sec. VII summarizes our new results.

II. EXPERIMENTAL OBSERVABLES

Existing measurements for anisotropic flow observables provide an estimate of the average value of η/s of the QGP, both at RHIC and LHC energies. What remains uncertain is how the η/s of the QGP depends on temperature (T). The temperature dependence of η/s of the QGP was discussed in Ref. [28]. The effects on hadron spectra and elliptic flow were studied in Ref. [59] for different parametrizations of $\eta/s(T)$. A more systematic study with event-by-event Eskola-Kajantie-Ruuskanen-Tuominen (EKRT) + viscous hydrodynamic calculations was recently initiated in Ref. [45], where the first (and only rather qualitative) possibilities were investigated (see Fig. 1 therein). The emerging picture is that the study of individual flow harmonics v_n alone is unlikely to reveal the details of the temperature dependence of η/s. It was already demonstrated in Ref. [45] that different $\eta/s(T)$ parametrizations can lead to the same centrality dependence of individual flow harmonics. In Ref. [36] new flow observables were introduced which quantify the degree of correlation between amplitudes of two different harmonics v_m and v_n. These new observables have the potential to discriminate between the contributions to anisotropic flow development from initial conditions and from the transport properties of the QGP [36]. Therefore, their measurement would provide experimental constraints on theoretical parameters used to describe the individual stages of the heavy-ion system evolution. In addition, it turned out that correlations of different flow harmonics are sensitive to

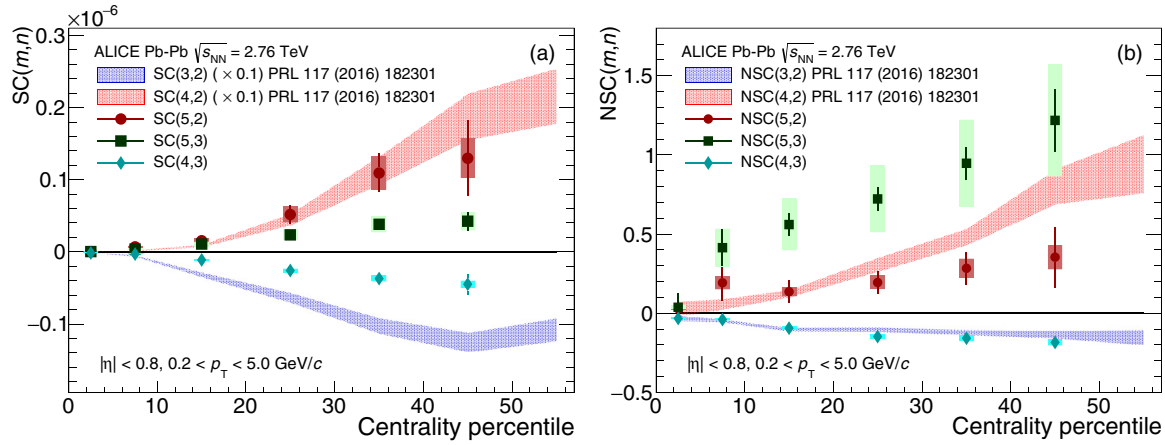

FIG. 1. The centrality dependence of SC(m,n) (a) and NSC(m,n) (b) with flow harmonics for $m = 3-5$ and $n = 2,3$ in Pb-Pb collisions at $\sqrt{s_{NN}} = 2.76$ TeV. The lower order harmonic correlations [SC(3,2), SC(4,2), NSC(3,2), and NSC(4,2)] are taken from Ref. [57] and shown as bands. The systematic and statistical errors are combined in quadrature for these lower order harmonic correlations. The SC(4,2) and SC(3,2) are downscaled by a factor of 0.1. Systematic uncertainties are represented with boxes for higher order harmonic correlations.

the temperature dependence of η/s [57], to which individual flow harmonics are weakly sensitive [45].

For reasons discussed in Refs. [57,60], the correlations between different flow harmonics cannot be studied experimentally with the set of observables introduced in Ref. [36]. Based on Ref. [60], new flow observables obtained from multiparticle correlations, *symmetric cumulants* (SC), were introduced.

The SC observables are defined as

$$\begin{aligned}\mathrm{SC}(m,n) &\equiv \langle\langle\cos(m\varphi_1+n\varphi_2-m\varphi_3-n\varphi_4)\rangle\rangle_c \\ &= \langle\langle\cos(m\varphi_1+n\varphi_2-m\varphi_3-n\varphi_4)\rangle\rangle \\ &\quad - \langle\langle\cos[m(\varphi_1-\varphi_2)]\rangle\rangle\langle\langle\cos[n(\varphi_1-\varphi_2)]\rangle\rangle \\ &= \langle v_m^2 v_n^2\rangle - \langle v_m^2\rangle\langle v_n^2\rangle, \end{aligned} \tag{3}$$

with the condition $m \neq n$ for two positive integers m and n (for details see Sec. IV C in Ref. [60]). In this article, SC(m,n) normalized by the product $\langle v_m^2\rangle\langle v_n^2\rangle$ [57,61] is denoted by NSC(m,n):

$$\mathrm{NSC}(m,n) \equiv \frac{\mathrm{SC}(m,n)}{\langle v_m^2\rangle\langle v_n^2\rangle}. \tag{4}$$

Normalized symmetric cumulants reflect only the strength of the correlation between v_m and v_n, while SC(m,n) has contributions from both the correlations between the two different flow harmonics and the individual harmonics. In Eq. (4) the products in the denominator are obtained from two-particle correlations using a pseudorapidity gap of $|\Delta\eta| > 1.0$ which suppresses biases from few-particle nonflow correlations. For the two two-particle correlations which appear in the definition of SC(m,n) in Eq. (3), the pseudorapidity gap is not needed, since nonflow is suppressed by construction in this observable. This was verified by HIJING model simulations in Ref. [57].

The ALICE measurements [57] have revealed that fluctuations of v_2 and v_3 are anticorrelated, while fluctuations of v_2 and v_4 are correlated for all centralities [57]. It was found that the details of the centrality dependence differ in the fluctuation-dominated (most central) and the geometry-dominated (mid-central) regimes [57]. The observed centrality dependence of SC(4,2) cannot be captured by models with constant η/s, indicating that the temperature dependence of η/s plays an important role. These results were also used to discriminate between different parametrizations of initial conditions. It was demonstrated that in the fluctuation-dominated regime (central collisions), Monte Carlo (MC)–Glauber initial conditions with binary collision weights are favored over wounded nucleon weights [57]. The first theoretical studies of SC observables can be found in Refs. [58,61–65].

III. DATA ANALYSIS

The data sample of Pb-Pb collisions at the center-of-mass energy $\sqrt{s_{NN}} = 2.76$ TeV analyzed in this article was recorded by ALICE during the 2010 heavy-ion run of the LHC. Detailed descriptions of the ALICE detector can be found in Refs. [66–68]. The time projection chamber (TPC) was used to reconstruct charged particle tracks and measure their momenta with full azimuthal coverage in the pseudorapidity range $|\eta| < 0.8$. Two scintillator arrays (V0A and V0C) which cover the pseudorapidity ranges $-3.7 < \eta < -1.7$ and $2.8 < \eta < 5.1$ were used for triggering and the determination of centrality [69]. The trigger conditions and the event selection criteria are identical to those described in Refs. [8,69]. Approximately 10^7 minimum-bias Pb-Pb events with a reconstructed primary vertex within ± 10 cm from the nominal interaction point along the beam direction are selected. Only charged particles reconstructed in the TPC in $|\eta| < 0.8$ and $0.2 < p_T < 5$ GeV/c were included in the analysis. The charged track quality cuts described in Ref. [8] were applied to minimize contamination from secondary charged particles and fake tracks. The track reconstruction efficiency and contamination were estimated from HIJING Monte Carlo simulations [70] combined with a GEANT3 [71] detector model and were found to be independent of the collision centrality. The reconstruction efficiency increases with transverse momenta from 70% to 80% for particles with $0.2 < p_T < 1$ GeV/c and remains constant at $(80 \pm 5)\%$ for $p_T > 1$ GeV/c. The estimated contamination

by secondary charged particles from weak decays and photon conversions is less than 6% at $p_T = 0.2$ GeV/c and falls below 1% for $p_T > 1$ GeV/c. The p_T cutoff of 0.2 GeV/c reduces event-by-event biases due to small reconstruction efficiency at lower p_T, while the high p_T cutoff of 5 GeV/c reduces the effects of jets on the measured correlations. Reconstructed TPC tracks constrained to vertex are required to have at least 70 space points (out of a maximum of 159). Only tracks with a transverse distance of closest approach to the primary vertex less than 3 mm, both in the longitudinal and transverse directions, are accepted. This reduces the contamination from secondary tracks produced in the detector material, particles from weak decays, etc. Tracks with kinks (i.e., tracks that appear to change direction due to multiple scattering or $K^{\pm}$ decays) were rejected.

IV. SYSTEMATIC UNCERTAINTIES

The systematic uncertainties are estimated by varying the event and track selection criteria. All systematic checks described here are performed independently. The SC(m,n) values resulting from each variation are compared to ones from the default event and track selection described in the previous section, and differences are taken as the systematic uncertainty due to each individual source. The contributions from different sources were added in quadrature to obtain the total systematic uncertainty.

The event centrality was determined by the V0 detectors [72] with better than 2% resolution for the whole centrality range analyzed. The systematic uncertainty from the centrality determination was evaluated by using the TPC and silicon pixel detector (SPD) [73] detectors instead of the V0 detectors. The systematic uncertainty on the symmetric cumulants which arises from the centrality uncertainty is about 3% both for SC(5,2) and SC(4,3) and 8% for SC(5,3). As described in Sec. III, the reconstructed vertex position along the beam axis (z vertex) is required to be located within 10 cm of the nominal interaction to ensure uniform detector acceptance for tracks within $|\eta| < 0.8$. The systematic uncertainty from the z-vertex cut was estimated by reducing the z-vertex range to 8 cm and was found to be less than 3%.

The analyzed events were recorded with two settings of the magnet field polarity and the resulting data sets have almost equal numbers of events. Events with both magnet field polarities were used in the default analysis, and the systematic uncertainties were evaluated from the variation between each of the two magnetic field settings. The uncertainty due to the p_T dependence of the track reconstruction efficiency was also taken into account. Magnetic field polarity variation and reconstruction efficiency effects contribute less than 2% to the systematic uncertainty.

The systematic uncertainty due to the track reconstruction procedure was estimated from comparisons between results for the so-called standalone TPC tracks with the same parameters as described in Sec. III, and tracks from a combination of the TPC and the inner tracking system (ITS) detectors with tighter selection criteria. To avoid nonuniform azimuthal acceptance due to dead zones in the SPD, and to get the best transverse momentum resolution, a hybrid track selection utilizing SPD hits and/or ITS refit tracks combined with TPC information was used. Then each track reconstruction strategy was evaluated by varying the threshold on parameters used to select the tracks at the reconstruction level. A systematic difference of up to 12% was observed in SC(m,n) from the different track selections. In addition, we applied the like-sign technique to estimate nonflow contributions [8] to SC(m,n). The difference between results obtained by selecting all charged particles and results obtained after either selecting only positively or only negatively charged particles was the largest contribution to the systematic uncertainty and is about 7% for SC(4,3) and 20% for SC(5,3).

Another large contribution to the systematic uncertainty originates from azimuthal nonuniformities in the reconstruction efficiency. In order to estimate its effects, we use the AMPT model (see Sec. VI), which has a uniform distribution in azimuthal angle. Detector inefficiencies were introduced to mimic the nonuniform azimuthal distribution in the data. For the observables SC(5,2), SC(5,3), and SC(4,3), the variation due to nonuniform acceptance is about 9%, 17%, and 11%, respectively. Overall, the systematic uncertainties are larger for SC(5,3) and SC(5,2) than for the lower harmonics of SC(m,n). This is because v_n decreases with increasing n and becomes more sensitive to azimuthal modulation due to detector imperfections.

V. RESULTS

The centrality dependence of the higher order harmonic correlations [SC(4,3), SC(5,2), and SC(5,3)] are presented in Fig. 1 and compared to the lower order harmonic correlations [SC(3,2) and SC(4,2)], which were published in Ref. [57]. The correlation between v_3 and v_4 is negative, and similarly for v_3 and v_2, while the other correlations are all positive, which reveals that v_2 and v_5 as well as v_3 and v_5 are correlated like v_2 and v_4, while v_3 and v_4 are anticorrelated like v_3 and v_2.

The higher order flow harmonic correlations are much smaller compared to the lower order harmonic correlations. In particular, SC(5,2) is 10 times smaller than SC(4,2) and SC(4,3) is about 20 times smaller than SC(3,2).

Unlike SC(m,n), the NSC(m,n) results with the higher order flow harmonics show almost the same order of the correlation strength as the lower order flow harmonic correlations NSC(3,2) or NSC(4,2). This demonstrates the advantage of using the normalized SC observables in which the correlation strength between flow harmonics is not hindered by the differences in magnitudes of different flow harmonics. The NSC(4,3) magnitude is comparable to NSC(3,2) and one finds that a hierarchy, NSC(5,3) > NSC(4,2) > NSC(5,2), holds for the centrality range 20–50% within the errors as shown in Fig. 1(b). The SC(5,2) magnitude is larger than SC(5,3), but the normalized correlation between v_5 and v_3 is stronger than the normalized correlation between v_5 and v_2. These results indicate that the lower order harmonic correlations are larger than higher order harmonic correlations, not only because of the correlation strength itself but also because of the strength of the individual flow harmonics.

It can be seen in Fig. 1(a) that the lower order harmonic correlations as well as SC(5,2) increase nonlinearly toward

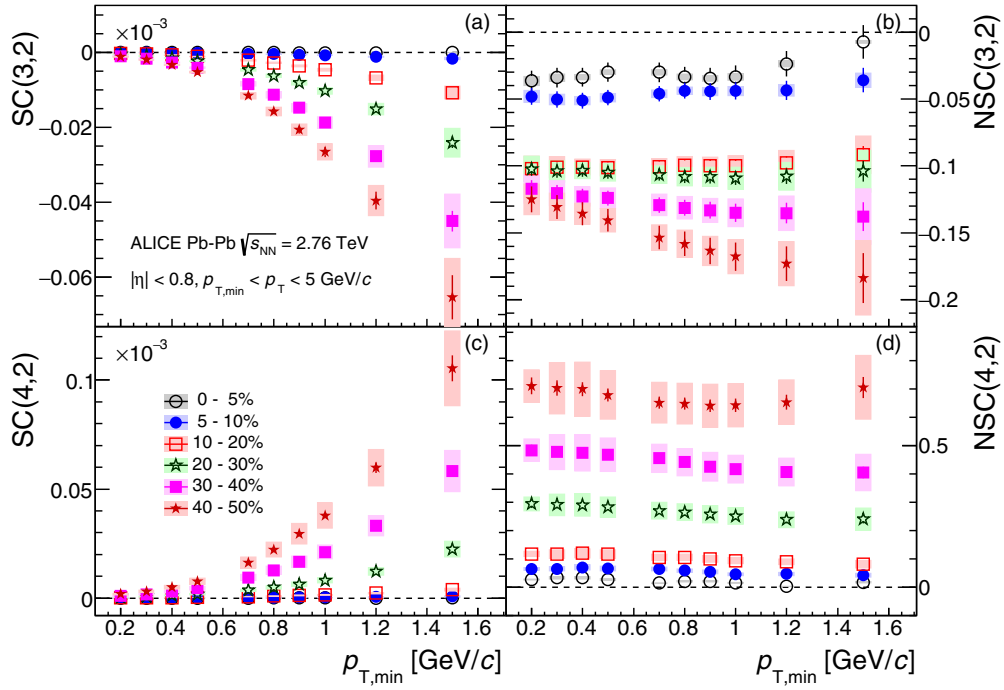

FIG. 2. SC(3,2) and SC(4,2) [panels (a) and (c)] as a function of minimum p_T cuts in Pb-Pb collisions at $\sqrt{s_{NN}} = 2.76$ TeV are shown in the left panels. The NSC(3,2) and NSC(4,2) [panels (b) and (d)] are shown in the right panels. Systematic uncertainties are represented with boxes.

peripheral collisions. In the case of SC(5,3) and SC(4,3), the centrality dependence is weaker than for the other harmonic correlations. The NSC(5,3) observable shows the strongest normalized correlation among all harmonics while NSC(5,2) shows the weakest centrality dependence. Both NSC(3,2) and NSC(4,3) are getting more anticorrelated toward peripheral collisions and have similar magnitudes.

To study the p_T dependence of SC(m,n), we present the results as a function of the low p_T cutoff ($p_{T,min}$), instead of using independent p_T intervals; this decreases large statistical fluctuations in the results. Various minimum p_T cuts from 0.2 to 1.5 GeV/c are applied. The p_T dependent results for SC(3,2) and SC(4,2) as a function of minimum p_T cuts are shown in Figs. 2(a) and 2(c). The strength of SC(m,n) becomes larger as $p_{T,min}$ increases. The centrality dependence is stronger with higher $p_{T,min}$ cuts, with SC(m,n) getting much larger as centrality percentile or $p_{T,min}$ increases. The NSC(3,2) and NSC(4,2) observables with different $p_{T,min}$ are shown in Figs. 2(b) and 2(d). The strong $p_{T,min}$ dependence observed in SC(m,n) is not seen in NSC(m,n). This indicates that the p_T dependence of SC(m,n) is dominated by the p_T dependence of the individual flow harmonics $\langle v_n \rangle$. The $p_{T,min}$ dependence of NSC(3,2) is not clearly seen and it is consistent with no $p_{T,min}$ dependence within the statistical and systematic errors for the centrality range 0–30%, while showing a moderate increase of anticorrelation with increasing $p_{T,min}$ for the 30–50% centrality range. The NSC(4,2) observable shows a moderate decreasing trend as $p_{T,min}$ increases. These observations are strikingly different from the p_T dependence of the individual flow harmonics, where the relative flow fluctuations $\sigma_{v_2}/\langle v_2 \rangle$ [74] are independent of transverse momentum up to p_T ~8 GeV/c (see Fig. 3 in Ref. [75]).

As discussed in Sec. II, the NSC(m,n) observables are normalized by the product $\langle v_m^2 \rangle \langle v_n^2 \rangle$. These products are obtained from two-particle correlations using a pseudorapidity gap of $|\Delta\eta| > 1.0$. In this paper, we denote the p_T integrated $v_n\{2, |\Delta\eta| > 1\}$ as v_n in the transverse momentum range $0.2 < p_T < 5.0$ GeV/c. The individual flow harmonics v_n used in calculations of the NSC observables are shown in Fig. 3. The centrality dependence of v_n for $n = 2-5$ is shown in Figs. 3(a)–3(c). The v_n values ($n < 5$) are equivalent to those in Ref. [11]. The fifth-order flow harmonic v_5 is shown in Fig. 3(c). The $p_{T,min}$ dependence of v_n for $n = 2-4$ is shown in Figs. 3(d)–3(f) in all centrality ranges relevant to the measured NSC(m,n) observables.

VI. MODEL COMPARISONS

We have performed a systematic comparison of the centrality and transverse momentum dependence of the SC(m,n) and NSC(m,n) to the event-by-event EKRT+viscous hydrodynamics [45], VISH2+1 [76,77], and the AMPT [63,78,79] models. Comparisons for v_n coefficients with the model calculations are presented in the Appendix.

In the event-by-event EKRT+viscous hydrodynamic calculations [45], the initial energy density profiles are calculated using a next-to-leading order perturbative-QCD + saturation model [80,81]. The subsequent space-time evolution is described by relativistic dissipative fluid dynamics with different parametrizations for the temperature dependence of the shear viscosity to entropy density ratio $\eta/s(T)$. This model gives a good description of the charged hadron multiplicity and the low-p_T region of the charged hadron spectra at RHIC and the LHC (see Figs. 11–13 in Ref. [45]). Each of the $\eta/s(T)$

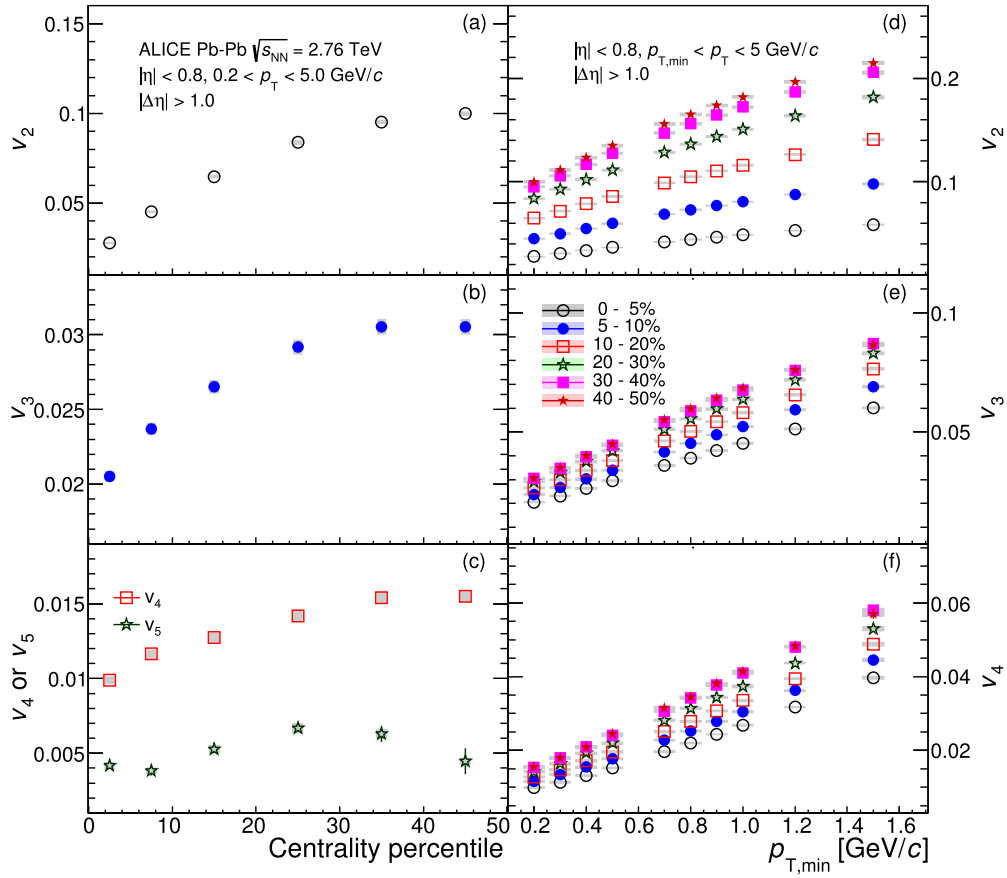

FIG. 3. The individual flow harmonics v_n for $n = 2-5$ in Pb-Pb collisions at $\sqrt{s_{NN}} = 2.76$ TeV are shown in the left panels [(a), (b), and (c)]. v_4 and v_5 are shown in the same panel (c). The $p_{T,min}$ dependence of v_n for $n = 2-4$ is shown in the right panels [(d), (e), and (f)].

parametrizations is adjusted to reproduce the measured v_n from central to midperipheral collisions (see Fig. 15 in Ref. [45] and our Appendix).

The VISH2+1 [76,77] event-by-event calculations for relativistic heavy-ion collisions are based on (2+1)-dimensional viscous hydrodynamics which describes the QGP phase and the highly dissipative and off-equilibrium late hadronic stages with fluid dynamics. By tuning transport coefficients and decoupling temperature for a given scenario of initial conditions, it can describe the p_T spectra and different flow harmonics at RHIC and the LHC [20,76,82,83] energies. Three different types of initial conditions [58] (MC-Glauber, Monte Carlo Kharzeev-Levin-Nardi (MC-KLN), and AMPT) along with different constant η/s values have been used for our data to model comparisons. Traditionally, the Glauber model constructs the initial entropy density from the wounded nucleon and binary collision density profiles [84]. The KLN model assumes that the initial energy density is proportional to that of the initial gluons calculated from the corresponding k_T factorization formula [85]. In Monte Carlo versions MC-Glauber and MC-KLN [86–88] of these models, additional initial state fluctuations are introduced through position fluctuations of individual nucleons inside the colliding nuclei. For the AMPT initial conditions [83,89,90], the fluctuating energy density profiles are constructed from the energy distribution of individual partons, which fluctuate in both momentum and coordinate space. Compared with the MC-Glauber and MC-KLN initial conditions, the additional Gaussian smearing in the AMPT initial conditions gives rise to nonvanishing initial local flow velocities [89].

Even though thermalization could be achieved quickly in collisions of very large nuclei and/or at extremely high energy [91], the dense matter created in heavy-ion collisions may not reach full thermal or chemical equilibrium due to its finite size and short lifetime. To address such nonequilibrium many-body dynamics, the AMPT model [78,92,93] has been developed, which includes both initial partonic and final hadronic interactions and the transition between these two phases of matter. The initial conditions in the AMPT are given by the spatial and momentum distributions of minijets and soft strings from the HIJING model [70,94]. For the data comparisons, three different configurations of the AMPT model have been used: the default one and string melting with and without hadronic rescattering. The input parameters used in all configurations are $\alpha_s = 0.33$ and a partonic cross section of 1.5 mb. In the default configuration, partons are recombined with their parent strings when they stop interacting. The resulting strings are later converted into hadrons using the Lund string fragmentation model [95,96]. The Lund string fragmentation parameters were set to $\alpha = 0.5$

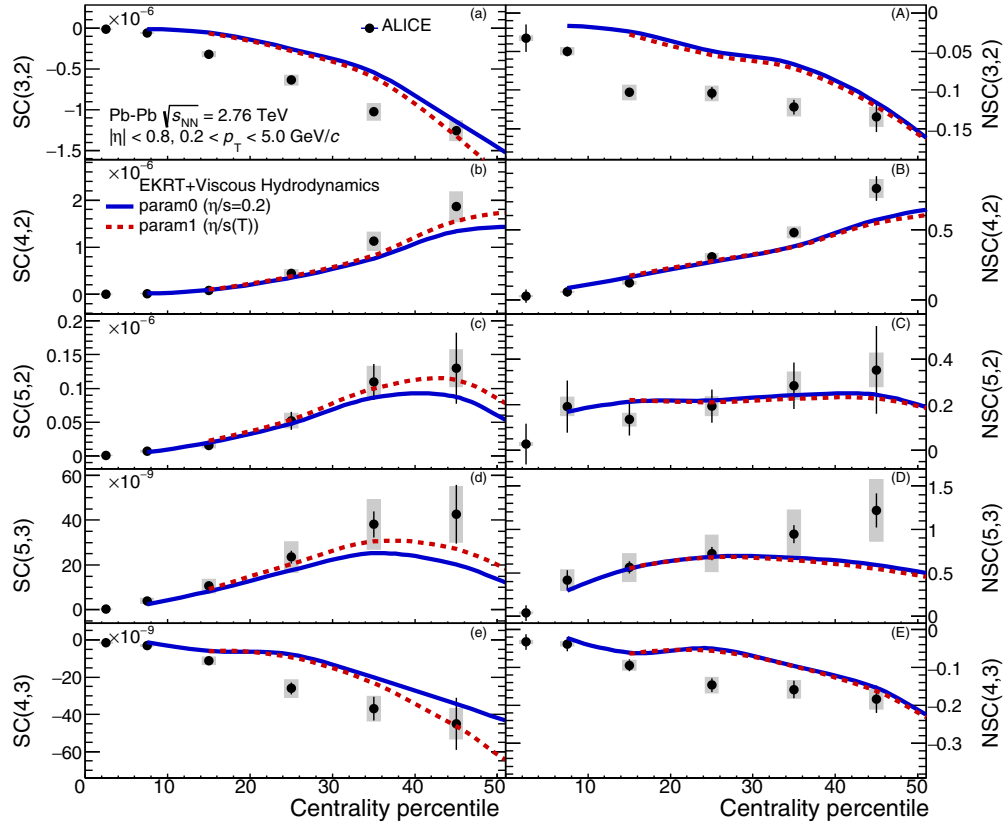

FIG. 4. The centrality dependence of SC(m,n) and NSC(m,n) in Pb-Pb collisions at $\sqrt{s_{NN}} = 2.76$ TeV. Results are compared to the event-by-event EKRT+viscous hydrodynamic calculations [45]. The lines are hydrodynamic predictions with two different $\eta/s(T)$ parametrizations. Left (right) panels show SC(m,n) (NSC(m,n)).

and $b = 0.9$ GeV^{-2}. In the string melting configuration, the initial strings are melted into partons whose interactions are described by the Zhang's parton cascade (ZPC) model [97]. These partons are then combined into the final-state hadrons via a quark coalescence model. In both configurations, the dynamics of the subsequent hadronic matter is described by a hadronic cascade based on a relativistic transport (ART) model [98] which includes resonance decays. The string melting configuration of the AMPT without hadronic rescattering was used to study the influence of the hadronic phase on the development of the anisotropic flow. Even though the string melting version of AMPT [78,99] reasonably well reproduces particle yields, p_T spectra, and v_2 of low-p_T pions and kaons in central and midcentral Au-Au collisions at $\sqrt{s_{NN}} = 200$ GeV and Pb-Pb collisions at $\sqrt{s_{NN}} = 2.76$ TeV [79], it was observed in a recent study [100] that it fails to quantitatively reproduce the flow harmonics of identified hadrons (v_2, v_3, v_4, and v_5) at $\sqrt{s_{NN}} = 2.76$ TeV. It turns out that the radial flow in AMPT is 25% lower than that measured at the LHC, which is responsible for this quantitative disagreement [100]. The details of the AMPT configurations used in this article and the comparisons of p_T-differential v_n for pions, kaons, and protons to the data can be found in Ref. [100].

A. Centrality dependence of SC(m,n) and NSC(m,n)

Comparison to event-by-event EKRT+viscous hydrodynamic predictions with various parametrizations of the temperature dependence of $\eta/s(T)$ was shown in Fig. 2 of Ref. [57]. It was demonstrated that NSC(3,2) is sensitive mainly to the initial conditions, while NSC(4,2) is sensitive to both the initial conditions and the system properties, which is consistent with the predictions from Ref. [36]. The model calculations for NSC(4,2) observable show that it has better sensitivity for different $\eta/s(T)$ parametrizations but they cannot describe either the centrality dependence or the absolute values. The discrepancy between data and theoretical predictions indicates that the current understanding of initial conditions in models of heavy-ion collisions needs to be revisited to further constrain $\eta/s(T)$. The measurement of SC(m,n) and NSC(m,n) can provide new constraints for the detailed modeling of fluctuating initial conditions.

The calculations for the two sets of parameters which describe the lower order harmonic correlations best are compared to the data in Fig. 4. As can be seen in Fig. 1 from Ref. [45], for the "param1" parametrization the phase transition from the hadronic to the QGP phase occurs at the lowest temperature, around 150 MeV. This parametrization is also characterized by a moderate slope in $\eta/s(T)$ which decreases (increases) in the hadronic (QGP) phase. The model calculations in which the temperature of the phase transition is larger than for "param1" are ruled out by the previous measurements [57]. While the correlations between v_5 and v_2 are well described at all centralities, the correlations between v_5 and v_3 are reproduced in the 0–40% centrality range and deviate by about one σ for

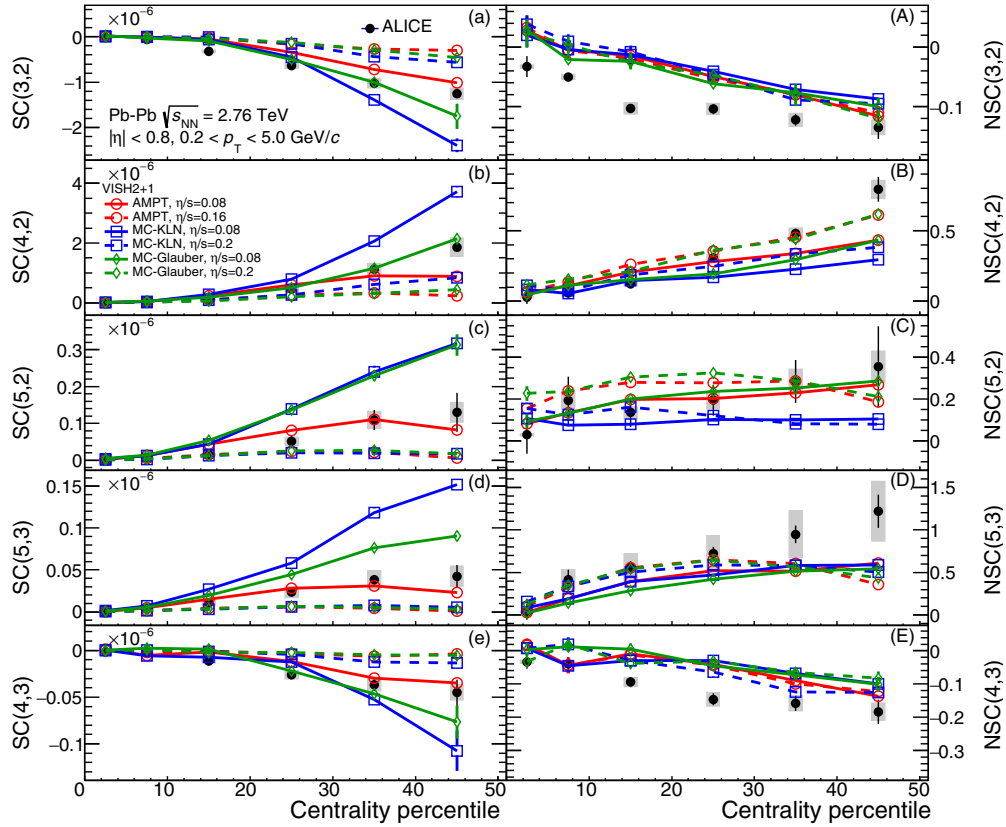

FIG. 5. The centrality dependence of SC(m,n) and NSC(m,n) in Pb-Pb collisions at $\sqrt{s_{NN}} = 2.76$ TeV. Results are compared to various VISH2+1 calculations [58]. Three initial conditions from AMPT, MC-KLN, and MC-Glauber are drawn as different colors and markers. The η/s parameters are shown as different line styles, the small shear viscosity ($\eta/s = 0.08$) are shown as solid lines, and large shear viscosities ($\eta/s = 0.2$ for MC-KLN and MC-Glauber and 0.16 for AMPT) are drawn as dashed lines. Left (right) panels show SC(m,n) (NSC(m,n)).

40–50% centrality. In the case of v_4 and v_3, the same models underestimate the anticorrelation in the data significantly in midcentral collisions and fail similarly for the anticorrelation between v_3 and v_2.

The comparison to the VISH2+1 calculation [58] is shown in Fig. 5. All calculations with large η/s regardless of the initial conditions ($\eta/s = 0.2$ for MC-KLN and MC-Glauber initial conditions and $\eta/s = 0.16$ for AMPT initial conditions) fail to describe the centrality dependence of the SC(m,n) observables of all orders, shown in the left panels in Fig. 5. Among the calculations with small η/s ($\eta/s = 0.08$), the one with the AMPT initial conditions describes the data better than the ones with other initial conditions for all SC(m,n) observables measured, but it cannot describe the data quantitively for most of the centrality ranges.

However, NSC(4,2) is sensitive both to the initial conditions and the η/s parametrizations used in the models. Even though NSC(4,2) favors both AMPT initial conditions with $\eta/s = 0.08$ and MC-Glauber initial conditions with $\eta/s = 0.20$, SC(4,2) can only be described by models with smaller η/s. Hence the calculation with large $\eta/s = 0.20$ is ruled out. We conclude that η/s should be small and that AMPT initial conditions are favored by the data. The NSC(5,2) and NSC(5,3) observables are quite sensitive to both the initial conditions and the η/s parametrizations. The SC(4,3) results clearly favor smaller η/s values but NSC(4,3) cannot be described by these models quantitively.

The SC(m,n) and NSC(m,n) observables calculated from AMPT simulations are compared with data in Fig. 6. For SC(3,2), the calculation with the default AMPT settings is closest to the data, but none of the AMPT configurations can describe the data fully. The third version based on the string melting configuration without the hadronic rescattering phase is also shown. The hadronic rescattering stage makes both SC(3,2) and NSC(3,2) smaller in the string melting AMPT model but not enough to describe the data. Further investigations proved why the default AMPT model can describe NSC(3,2) but underestimates SC(3,2). By taking the differences in the individual flow harmonics (v_2 and v_3) between the model and data into account, it was possible to recover the difference in SC(3,2) between the data and the model. The discrepancy in SC(3,2) can be explained by the overestimated individual v_n values as reported in Ref. [100] in all centrality ranges.

In the case of SC(4,2), the string melting configuration of the AMPT model can describe the data fairly well while the default configuration underestimates it. The NSC(4,2) observable is slightly overestimated by the string melting setting which can describe SC(4,2) but the default AMPT configuration can describe the data better. The influence of the hadronic rescattering

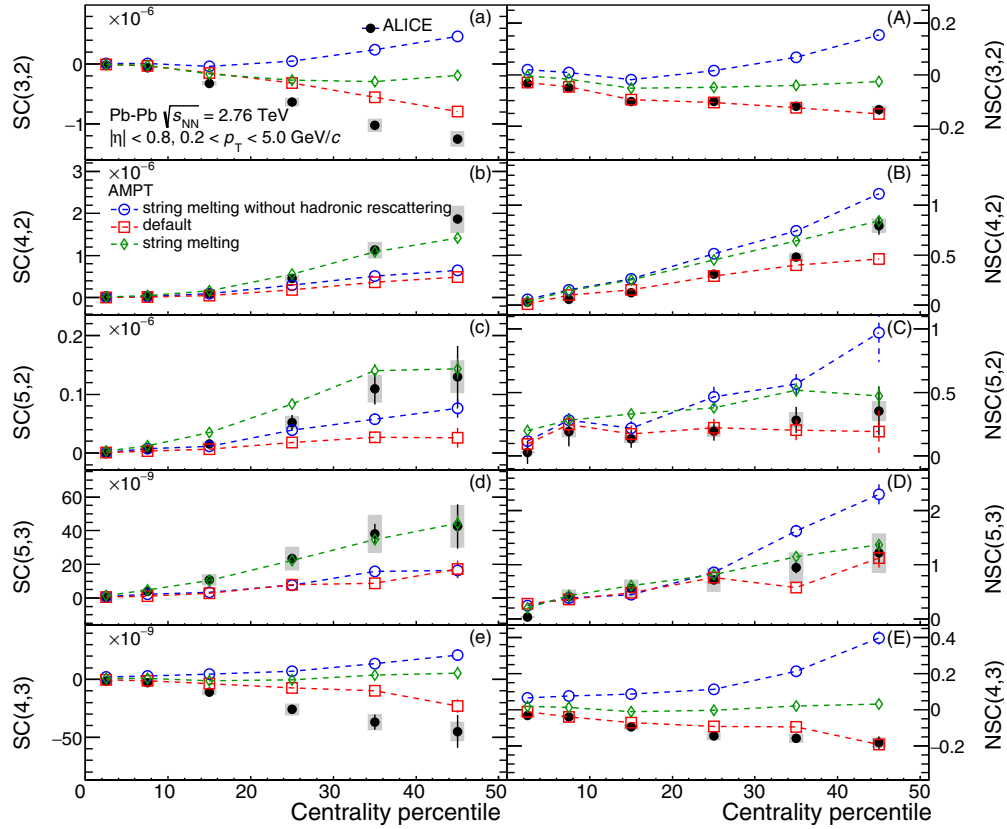

FIG. 6. The centrality dependence of SC(m,n) and NSC(m,n) in Pb-Pb collisions at $\sqrt{s_{NN}} = 2.76$ TeV. Results are compared to various AMPT models. Left (right) panels show SC(m,n) (NSC(m,n)).

phase on NSC(4,2) is opposite to other observables [SC(3,2), NSC(3,2), and SC(4,2)]. The hadronic rescattering makes NSC(4,2) slightly smaller. It should be noted that the agreement with SC(m,n) should not be overemphasized since there are discrepancies in the individual v_n between the AMPT models and the data as was demonstrated for SC(3,2). Hence, the simultaneous description of SC(m,n) and NSC(m,n) should give better constraints on the parameters in AMPT models. The string melting AMPT model describes SC(5,3) and NSC(5,3) well. However, the same setting overestimates SC(5,2) and NSC(5,2). The default AMPT model can describe NSC(5,3) and NSC(5,2) fairly well, as in the case of NSC(3,2) and NSC(4,2). In the case of SC(4,3), neither of the settings can describe the data but the default AMPT model comes the closest to the data. The NSC(4,3) observable is well described by the default AMPT model but cannot be reproduced by the string melting AMPT model. In summary, the default AMPT model describes well the normalized symmetric cumulants [NSC(m,n)] from lower to higher order harmonic correlations while the string melting AMPT model overestimates NSC(3,2) and NSC(5,2) and predicts a very weak correlation both for NSC(3,2) and NSC(4,3).

As discussed in Sec. V, a hierarchy NSC(5,3) > NSC(4,2) > NSC(5,2) holds for centrality ranges >20% within the errors. Except for the 0–10% centrality range, we found that the same hierarchy also holds in the hydrodynamic calculations and the AMPT models explored in this article. While NSC(5,2) is smaller than NSC(5,3), SC(5,2) is larger than SC(5,3). The observed inverse hierarchy, SC(5,2) > SC(5,3), can be explained by different magnitudes of the individual flow harmonics ($v_2 > v_3$). This can be attributed to the fact that flow fluctuations are stronger for v_3 than v_2 [14]. This was claimed in Ref. [58] and also seen in Ref. [101] based on the AMPT model calculations. NSC(m,n) correlators increase with larger η/s in hydrodynamic calculations in the 0–30% centrality range in the same way as the event plane correlations [102,103]. In semiperipheral collisions (>40%), the opposite trend is observed.

We list here the important findings from the model comparisons to the centrality dependence of SC(m,n) and NSC(m,n):

(i) The NSC(3,2) observable is sensitive mainly to the initial conditions, while the other observables are sensitive to both the initial conditions and the temperature dependence of η/s.
(ii) The correlation strength between v_3 and v_2 and between v_4 and v_3 [SC(3,2), SC(4,2), NSC(3,2), and NSC(4,3)] is significantly underestimated in hydrodynamic model calculations in midcentral collisions.
(iii) All the VISH2+1 model calculations with large η/s fail to describe the centrality dependence of the correlations regardless of the initial conditions.
(iv) Among the VISH2+1 model calculations with small η/s ($\eta/s = 0.08$), the one with the AMPT initial conditions describes the data qualitatively but not quantitively for most of the centrality ranges.

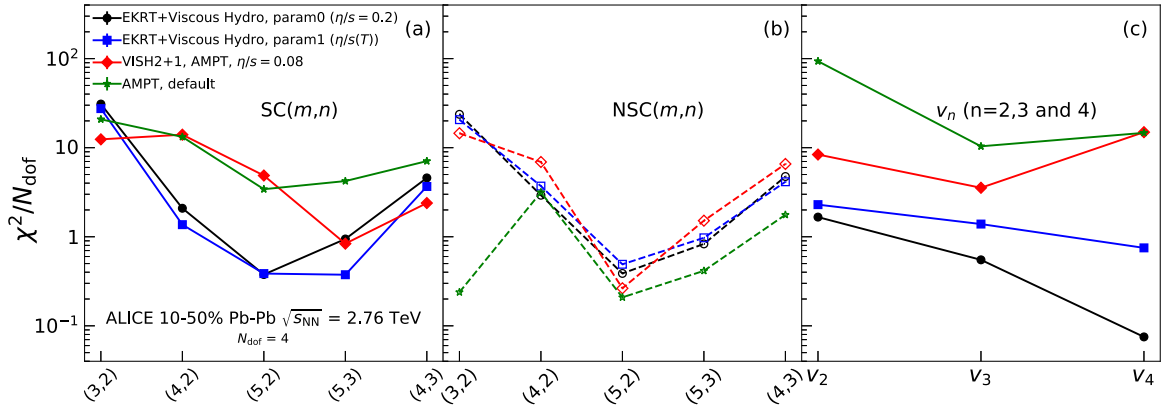

FIG. 7. The $\chi^2/N_{\rm dof}$ values calculated by Eq. (5) are shown for SC(m,n) (a), NSC(m,n) (b), and individual harmonics v_n (c). Results are for model calculations which are best in describing the SC observables for each of the three different types of models.

(v) The default AMPT model can describe the normalized symmetric cumulants [NSC(m,n)] quantitively for most centralities while the string melting AMPT model fails to describe them.

(vi) A hierarchy NSC(5,3) > NSC(4,2) >NSC(5,2) holds for centrality percentile ranges >20% within the errors. This hierarchy is reproduced well both by hydrodynamic and AMPT model calculations.

The agreement of various model calculations with the data is quantified by calculating the $\chi^2/N_{\rm dof}$,

$$\chi^2/N_{\rm dof} = \frac{1}{N_{\rm dof}} \sum_{i=1}^{N_{\rm dof}} \frac{(y_i - f_i)^2}{\sigma_i^2}, \tag{5}$$

where y_i (f_i) is a measurement (model) value in a centrality bin i. The systematic and statistical errors from the data are combined in quadrature $\sigma_i = \sqrt{\sigma_{i,\rm stat}^2 + \sigma_{i,\rm syst}^2 + \sigma_{f_i,\rm stat}^2}$ together with the statistical errors of the model calculations. The total number of data samples $N_{\rm dof}$ in Eq. (5) is 4, which corresponds to the number of bins in the centrality range 10–50% used in $\chi^2/N_{\rm dof}$ calculations. The $\chi^2/N_{\rm dof}$ for model calculations which are best in describing the SC observables for each of the three different types of models are shown in Fig. 7.

The results for SC(m,n) and NSC(m,n) are presented in Figs. 7(a) and 7(b), respectively. The $\chi^2/N_{\rm dof}$ values for the individual flow harmonics v_n for $n = 2-4$ are shown in Fig. 7(c). We found that in the case of the calculations from VISH2+1 with AMPT initial conditions ($\eta/s = 0.08$) and the default configuration of the AMPT model, the $\chi^2/N_{\rm dof}$ values for SC(m,n) are larger than those for NSC(m,n). This reflects the fact that the individual flow harmonics v_n are not well described by those models compared to event-by-event EKRT+viscous hydrodynamics. This is quantified in Fig. 7(c), where the $\chi^2/N_{\rm dof}$ values for v_n are much larger both for VISH2+1 and default AMPT calculations than event-by-event EKRT+viscous hydrodynamics. The default configuration of the AMPT model gives the best $\chi^2/N_{\rm dof}$ values for NSC(m,n), especially for NSC(3,2). However, the $\chi^2/N_{\rm dof}$ values of this model are largest for v_n among the models especially for v_2.

The $\chi^2/N_{\rm dof}$ values for v_2 and v_3 are significantly smaller than those for SC(3,2) and NSC(3,2) for all the hydrodynamic calculations. The $\chi^2/N_{\rm dof}$ values for SC(4,2) and NSC(4,2) from event-by-event EKRT+viscous hydrodynamics are comparable to that for v_2 but larger than for v_4. The $\chi^2/N_{\rm dof}$ for calculations for v_n with constant $\eta/s = 0.20$ ("param0") are smaller than those with temperature-dependent η/s parametrization with a minimal value of $\eta/s = 0.12$ at the temperature around 150 MeV ("param1"), while an opposite trend is observed for SC(m,n), in particular for SC(4,2) and SC(5,3). This illustrates that a combination of the SC(m,n) observables with the individual flow harmonics v_n may provide sensitivity to the temperature dependence of the $\eta/s(T)$ and together they allow for better constraints of the model parameters.

Even though the calculations from event-by-event EKRT+viscous hydrodynamics give the best $\chi^2/N_{\rm dof}$ values for both SC(m,n) and NSC(m,n), the $\chi^2/N_{\rm dof}$ values are large, especially for the observables which include v_3. Even with the best model calculations, the $\chi^2/N_{\rm dof}$ value varies a lot depending on the model parameters and/or different order SC observables, which implies that the different order harmonic correlations have different sensitivity to the initial conditions and the system properties.

B. Transverse momentum dependence of correlations between v_2 and v_3 and between v_2 and v_4

The NSC(3,2) and NSC(4,2) observables as a function of $p_{\rm T,min}$ are compared to the AMPT simulations in Figs. 8 and 9, respectively. The observed $p_{\rm T}$ dependence for NSC(3,2) in midcentral collisions is also seen in AMPT simulations for higher $p_{\rm T,min}$. The default configuration of the AMPT reproduces NSC(3,2), while the other AMPT configurations predict a very strong $p_{\rm T}$ dependence above 1 GeV/c and cannot describe the magnitudes of both NSC(3,2) and NSC(4,2) simultaneously. In the case of NSC(3,2), the default AMPT model describes the magnitude and $p_{\rm T}$ dependence well in all collision centralities except for 40–50%, where the model underestimates the data and shows a stronger $p_{\rm T}$ dependence than the data. As for NSC(4,2), the default AMPT configuration which describes NSC(3,2) can also reproduce the

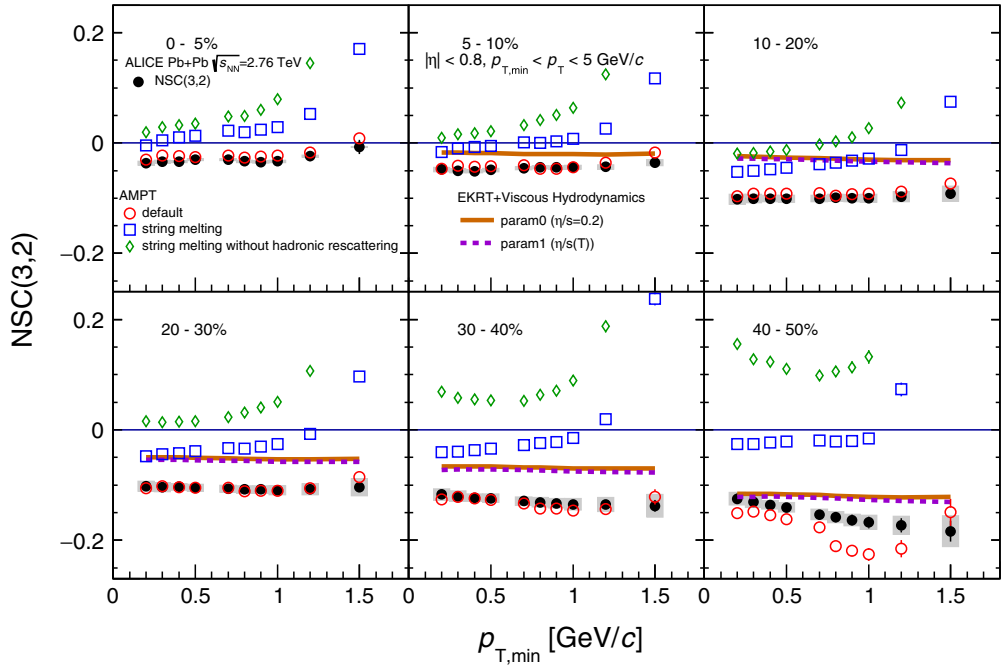

FIG. 8. NSC(3,2) as a function of the minimum p_T cut in Pb-Pb collisions at $\sqrt{s_{NN}} = 2.76$ TeV. Results are compared to various AMPT configurations and event-by-event EKRT+viscous hydrodynamic calculations [45].

data well except for the 10–20% and 40–50% centralities. Comparison of the string melting AMPT configuration with and without hadronic rescattering suggests that a very strong p_T dependence as well as the correlation strength are weakened by the hadronic rescattering. Consequently, the observed weak p_T dependence may be due to hadronic rescattering. The relative contributions to the final-state particle distributions from partonic and hadronic stages need further study.

The event-by-event EKRT+viscous hydrodynamic calculations are also compared to the data in Figs. 8 and 9. In the case of NSC(3,2), the hydrodynamic calculations underestimate the magnitude of the data as discussed in Sec. VI A

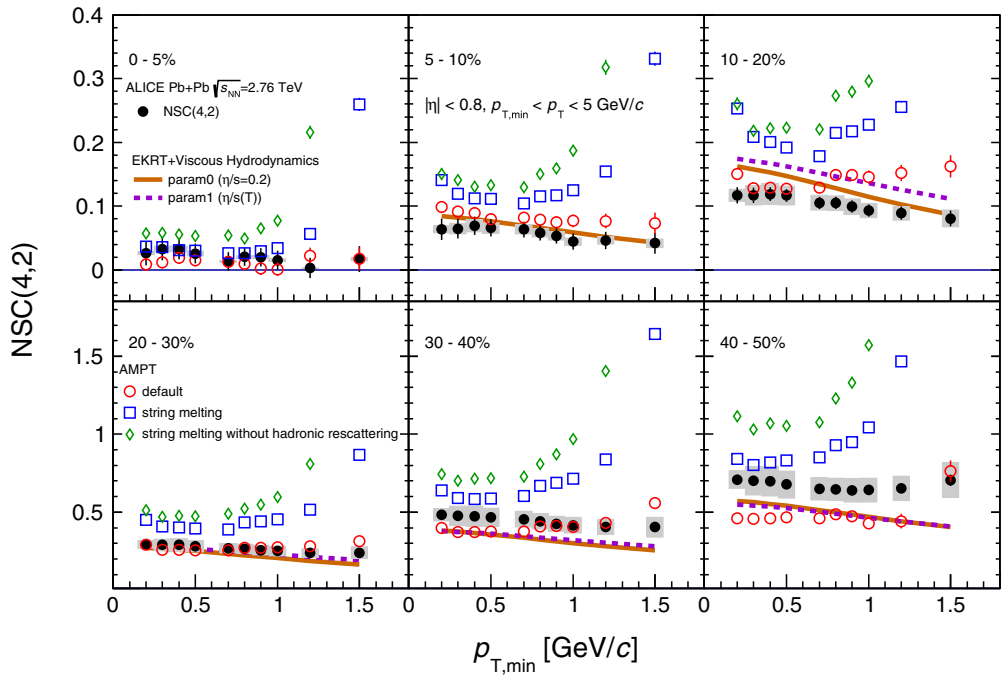

FIG. 9. NSC(4,2) as a function of the minimum p_T cut in Pb-Pb collisions at $\sqrt{s_{NN}} = 2.76$ TeV. Results are compared to various AMPT configurations and event-by-event EKRT+viscous hydrodynamic calculations [45].

and show very weak p_{T} dependence for all centralities. The p_{T} dependence of NSC(3,2) is well captured by the model calculations in all collision centralities except for 40–50%, where the data show stronger p_{T} dependence than the models. The difference between the model calculations with the two different parametrizations of $\eta/s(T)$ is very small. As for NSC(4,2), the model calculations overestimate the magnitude of the data in the 5–20% centrality range and underestimate it in the centrality range 30–50%. However, the p_{T} dependence is well described by the model calculations in all centrality ranges, while the difference of the model results for the two parametrizations in most centralities is rather small.

The observed moderate p_{T} dependence in midcentral collisions both for NSC(3,2) and NSC(4,2) might be an indication of possible viscous corrections to the equilibrium distribution at hadronic freeze-out, as predicted in Ref. [36]. The comparisons to hydrodynamic models can further help us to understand the viscous corrections to the momentum distributions at hadronic freeze-out [45,52,54–56].

VII. SUMMARY

In this article, we report the centrality dependence of correlations between the higher order harmonics (v_4, v_5) and the lower order harmonics (v_2, v_3) as well as the transverse momentum dependence of the correlations between v_3 and v_2 and between v_4 and v_2. The results are presented in terms of the symmetric cumulants SC(m,n). It was demonstrated earlier in Ref. [57] that SC(m,n) is insensitive to nonflow effects and independent of symmetry plane correlations.

We have found that fluctuations of SC(3,2) and SC(4,3) are anticorrelated in all centralities while fluctuations of SC(4,2), SC(5,2), and SC(5,3) are correlated for all centralities. These measurements were compared to various hydrodynamic model calculations with different initial conditions as well as different parametrizations of the temperature dependence of η/s. It is found that the different order harmonic correlations have different sensitivities to the initial conditions and the system properties. Therefore, they have discriminating power in separating the effects of η/s from the initial conditions on the final-state particle anisotropies. The comparisons to VISH2+1 calculations show that all the models with large η/s, regardless of the initial conditions, fail to describe the centrality dependence of higher order correlations. Based on the tested model parameters, the data favor small η/s and the AMPT initial conditions.

A quite clear separation of the correlation strength for different initial conditions is observed for these higher order harmonic correlations compared to the lower order. The default configuration of the AMPT model describes well the normalized symmetric cumulants [NSC(m,n)] for most centralities and for most combinations of harmonics which were considered. Finally, we have found that v_3 and v_2 as well as v_4 and v_2 correlations have moderate p_{T} dependence in midcentral collisions. This might be an indication of possible viscous corrections to the equilibrium distribution at hadronic freeze-out. Together with the measurements of individual harmonics, the new results for SC(m,n) and NSC(m,n) can be used to further optimize model parameters and put better constraints on the initial conditions and the transport properties of nuclear matter in ultrarelativistic heavy-ion collisions.

ACKNOWLEDGMENTS

The ALICE Collaboration would like to thank all its engineers and technicians for their invaluable contributions to the construction of the experiment and the CERN accelerator teams for the outstanding performance of the LHC complex. The ALICE Collaboration gratefully acknowledges the resources and support provided by all grid centers and the Worldwide LHC Computing Grid (WLCG) collaboration. The ALICE Collaboration acknowledges the following funding agencies for their support in building and running the ALICE detector: A. I. Alikhanyan National Science Laboratory (Yerevan Physics Institute) Foundation (ANSL), State Committee of Science and World Federation of Scientists (WFS), Armenia; Austrian Academy of Sciences and Nationalstiftung für Forschung, Technologie und Entwicklung, Austria; Ministry of Communications and High Technologies, National Nuclear Research Center, Azerbaijan; Conselho Nacional de Desenvolvimento Científico e Tecnológico (CNPq), Universidade Federal do Rio Grande do Sul (UFRGS), Financiadora de Estudos e Projetos (Finep), and Fundação de Amparo à Pesquisa do Estado de São Paulo (FAPESP), Brazil; Ministry of Science and Technology of China (MSTC), National Natural Science Foundation of China (NSFC), and Ministry of Education of China (MOEC), China; Ministry of Science, Education, and Sport and Croatian Science Foundation, Croatia; Ministry of Education, Youth, and Sports of the Czech Republic, Czech Republic; the Danish Council for Independent Research–Natural Sciences, the Carlsberg Foundation, and Danish National Research Foundation (DNRF), Denmark; Helsinki Institute of Physics (HIP), Finland; Commissariat à l'Energie Atomique (CEA), Institut National de Physique Nucléaire et de Physique des Particules (IN2P3), and Centre National de la Recherche Scientifique (CNRS), France; Bundesministerium für Bildung, Wissenschaft, Forschung und Technologie (BMBF) and GSI Helmholtzzentrum für Schwerionenforschung GmbH, Germany; General Secretariat for Research and Technology, Ministry of Education, Research, and Religions, Greece; National Research, Development, and Innovation Office, Hungary; Department of Atomic Energy Government of India (DAE) and Council of Scientific and Industrial Research (CSIR), New Delhi, India; Indonesian Institute of Science, Indonesia; Centro Fermi - Museo Storico della Fisica e Centro Studi e Ricerche Enrico Fermi and Istituto Nazionale di Fisica Nucleare (INFN), Italy; Institute for Innovative Science and Technology, Nagasaki Institute of Applied Science (IIST), Japan Society for the Promotion of Science (JSPS) KAKENHI, and Japanese Ministry of Education, Culture, Sports, Science, and Technology (MEXT), Japan; Consejo Nacional de Ciencia (CONACYT) y Tecnología, through Fondo de Cooperación Internacional en Ciencia y Tecnología (FONCICYT) and Dirección General de Asuntos del Personal Academico (DGAPA), Mexico; Nederlandse Organisatie voor Wetenschappelijk Onderzoek (NWO), Netherlands; the Research Council of Norway, Norway; Commission on Science and Technology for Sustainable Development in the

South (COMSATS), Pakistan; Pontificia Universidad Católica del Perú, Peru; Ministry of Science and Higher Education and National Science Centre, Poland; Korea Institute of Science and Technology Information and National Research Foundation of Korea (NRF), Republic of Korea; Ministry of Education and Scientific Research, Institute of Atomic Physics and Romanian National Agency for Science, Technology, and Innovation, Romania; Joint Institute for Nuclear Research (JINR), Ministry of Education and Science of the Russian Federation and National Research Centre Kurchatov Institute, Russia; Ministry of Education, Science, Research, and Sport of the Slovak Republic, Slovakia; National Research Foundation of South Africa, South Africa; Centro de Aplicaciones Tecnológicas y Desarrollo Nuclear (CEADEN), Cubaenergía, Cuba, Ministerio de Ciencia e Innovacion and Centro de Investigaciones Energéticas, Medioambientales y Tecnológicas (CIEMAT), Spain; Swedish Research Council (VR) and Knut and Alice Wallenberg Foundation (KAW), Sweden; European Organization for Nuclear Research, Switzerland; National Science and Technology Development Agency (NSDTA), Suranaree University of Technology (SUT) and Office of the Higher Education Commission under NRU project of Thailand, Thailand; Turkish Atomic Energy Agency (TAEK), Turkey; National Academy of Sciences of Ukraine, Ukraine; Science and Technology Facilities Council (STFC), United Kingdom; and National Science Foundation of the United States of America (NSF) and United States Department of Energy, Office of Nuclear Physics (DOE NP), United States of America.

APPENDIX: MODEL COMPARISONS OF THE INDIVIDUAL FLOW HARMONICS v_n

As discussed in Sec. II, NSC(m,n) is expected to be insensitive to the magnitudes of v_m and v_n but SC(m,n) has contributions from both the correlations between the two different flow harmonics and the individual harmonics v_n. Therefore, it is important to check how well the theoretical models used in Sec. VI describe the measured v_n data shown in Sec. V. v_n results presented in this section are for charged particles in the pseudorapidity range $|\eta| < 0.8$ and the transverse momentum range $0.2 < p_{\mathrm{T}} < 5.0$ GeV/c as a function of collision centrality [11].

The measured v_n for $n = 2{-}4$ in Pb-Pb collisions at $\sqrt{s_{NN}} = 2.76$ TeV are compared to the event-by-event EKRT+viscous hydrodynamic calculations [45] in Fig. 10. In these calculations, the initial conditions and η/s parametrizations are chosen to reproduce the LHC v_n data. The calculations capture the centrality dependence of v_n in the central and midcentral collisions within 5% for v_2 and 10% for v_3 and v_4.

The VISH2+1 calculations with various initial conditions and η/s parameters are compared to the v_n data in Fig. 11. Neither MC-Glauber nor MC-KLN initial conditions can simultaneously describe v_2, v_3, and v_4. In particular, for MC-Glauber initial conditions, VISH2+1 with $\eta/s = 0.08$ can describe well v_2 from central to midcentral collisions, but overestimates v_3 and v_4 for the same centrality ranges. For MC-KLN initial conditions, VISH2+1 with $\eta/s = 0.20$ reproduces v_2 but underestimates v_3 and v_4 for the presented centrality regions. The calculations with AMPT initial conditions improves the simultaneous descriptions of v_n ($n = 2$, 3, and 4). The overall difference to the data is quite large if all the model settings are considered, about 30% for v_n ($n = 2$ and 3) and 50% for v_4. The calculations with AMPT initial conditions reproduce the observed centrality dependence with an accuracy of 10–20%.

The AMPT calculations with various configurations are compared to the v_n data in Fig. 12. The string melting version of AMPT [78,99] reasonably reproduces v_n as shown in Fig. 12 within 20% for v_2 and 10% for v_3 and v_4. The version based on the string melting configuration without the hadronic rescattering phase underestimates the data compared to the

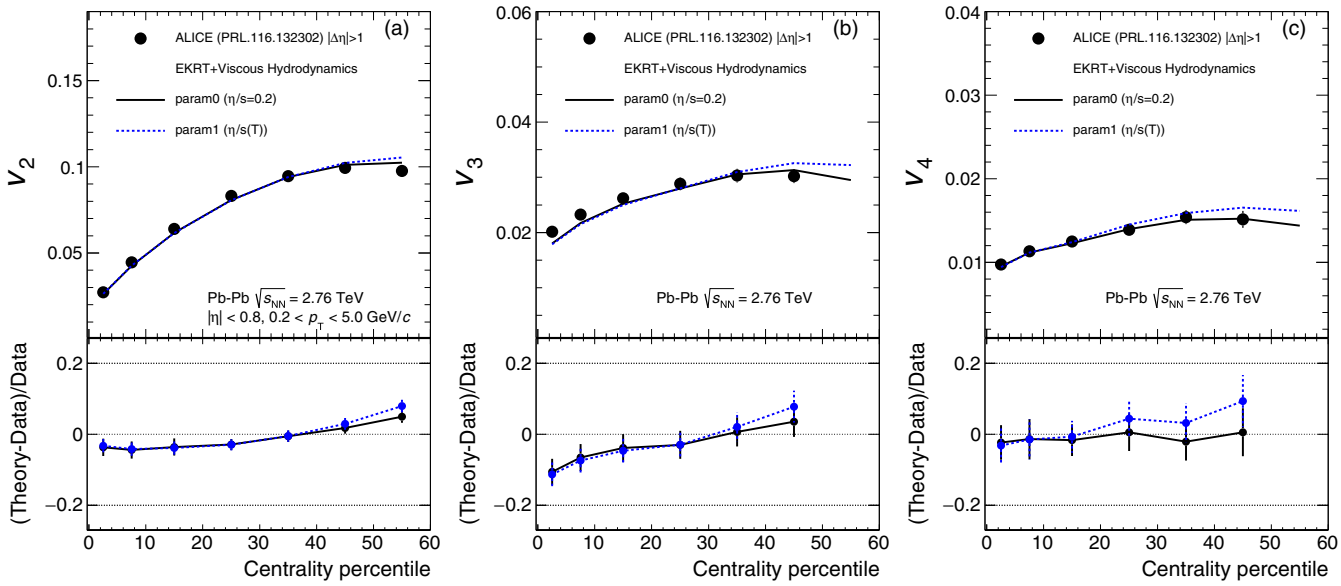

FIG. 10. The individual flow harmonics v_n for $n = 2{-}4$ in Pb-Pb collisions at $\sqrt{s_{NN}} = 2.76$ TeV [11]. Results are compared to the event-by-event EKRT+viscous hydrodynamic calculations [45] for two different $\eta/s(T)$ parametrizations, labeled in the same way as in Ref. [45].

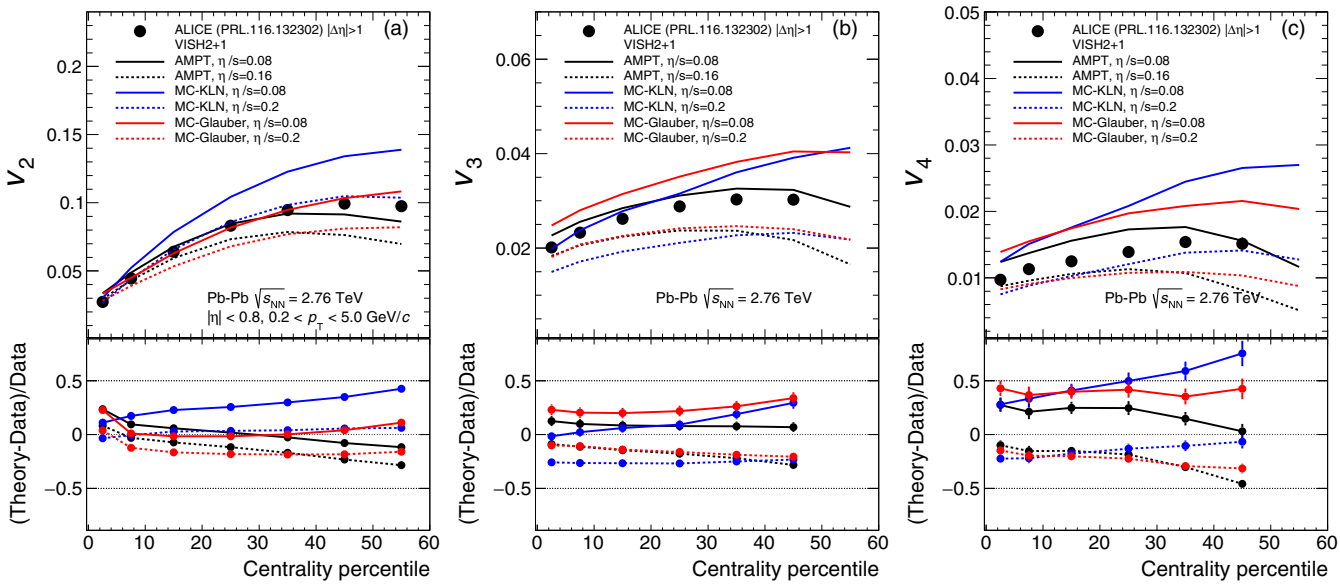

FIG. 11. The individual flow harmonics v_n for $n = 2{-}4$ in Pb-Pb collisions at $\sqrt{s_{NN}} = 2.76$ TeV [11]. Results are compared to various VISH2+1 calculations [58]. Three initial conditions from AMPT, MC-KLN, and MC-Glauber are shown in different colors. The results for different η/s values are shown as different line styles, the small shear viscosity ($\eta/s = 0.08$) are shown as solid lines, and large shear viscosities ($\eta/s = 0.2$ for MC-KLN and MC-Glauber and, 0.16 for AMPT) are drawn as dashed lines.

calculations with the string melting version of AMPT, which demonstrates that a large fraction of the flow is developed during the late hadronic rescattering stage in the string melting version of AMPT. The default version of AMPT underestimates v_n for $n = 2{-}4$ by $\approx$20%. It should be noted that the default AMPT model can describe the normalized symmetric cumulants [NSC(m,n)] quantitively for most centralities while the string melting AMPT model fails to describe them.

Finally, few selected calculations from three theoretical models which describe the v_n data best are shown in Fig. 13. The calculations from event-by-event EKRT+viscous hydrodynamics, VISH2+1 with AMPT initial conditions ($\eta/s = 0.08$) and the string melting version of AMPT give the best description of the individual flow harmonics v_n ($n = 2$, 3 and 4) with an accuracy of 5–20%. The centrality dependence differs in the three models as well as in the different order flow harmonics. Together with SC(m,n) and NSC(m,n), the simultaneous description of individual flow harmonics v_n at all orders is necessary to further optimize model parameters and put better constraints on the initial conditions and the transport properties of nuclear matter in ultrarelativistic heavy-ion collisions.

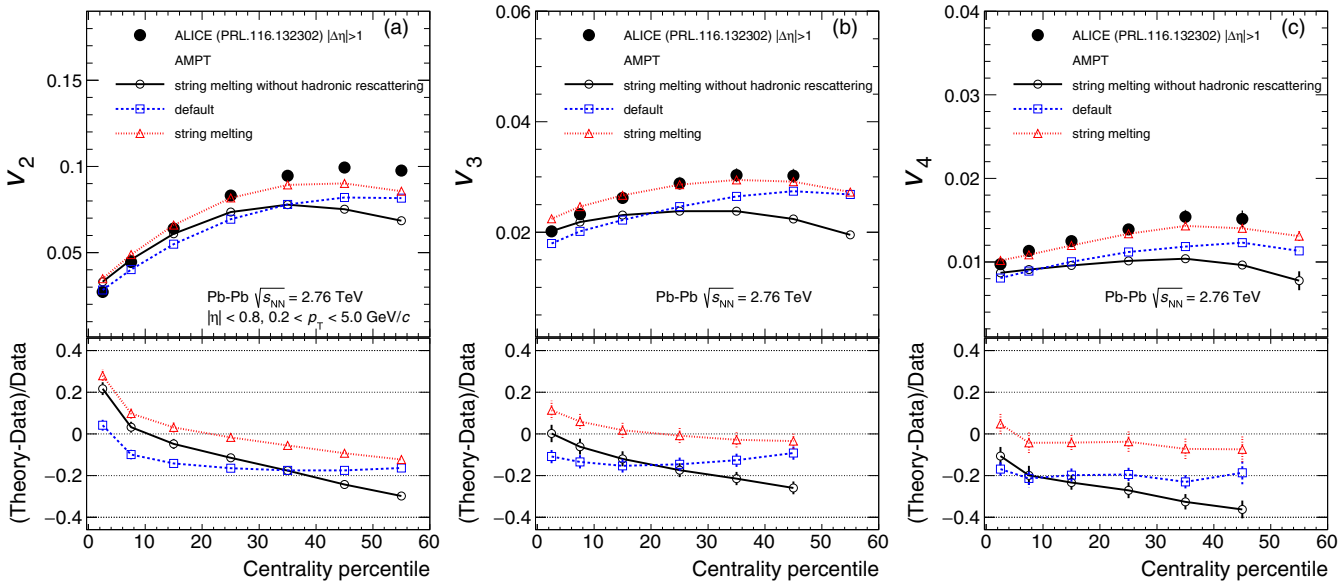

FIG. 12. The individual flow harmonics v_n ($n = 2$, 3, and 4) in Pb-Pb collisions at $\sqrt{s_{NN}} = 2.76$ TeV [11]. Results are compared to various AMPT models.

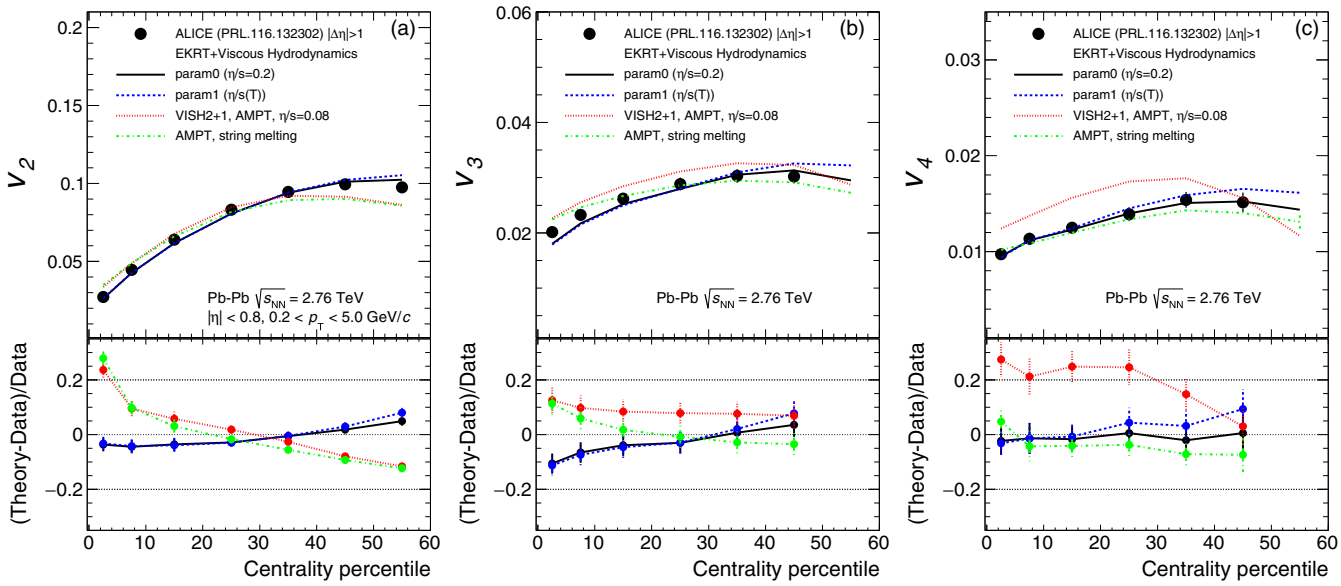

FIG. 13. The individual flow harmonics v_n for $n = 2-4$ in Pb-Pb collisions at $\sqrt{s_{NN}} = 2.76$ TeV [11]. Results are compared with selected calculations from three different types of models which are best in describing v_n coefficients.

[1] H. von Gersdorff, L. McLerran, M. Kataja, and P. V. Ruuskanen, Studies of the hydrodynamic evolution of matter produced in fluctuations in $p\overline{p}$ collisions and in ultrarelativistic nuclear collisions, Phys. Rev. D **34**, 794 (1986).

[2] U. Heinz and R. Snellings, Collective flow and viscosity in relativistic heavy-ion collisions, Annu. Rev. Nucl. Part. Sci. **63**, 123 (2013).

[3] K. H. Ackermann *et al.* (STAR Collaboration), Elliptic Flow in Au + Au Collisions at $\sqrt{s_{NN}} = 130$ GeV, Phys. Rev. Lett. **86**, 402 (2001).

[4] J. Adams *et al.* (STAR Collaboration), Experimental and theoretical challenges in the search for the quark gluon plasma: The STAR Collaboration's critical assessment of the evidence from RHIC collisions, Nucl. Phys. A **757**, 102 (2005).

[5] K. Adcox *et al.* (PHENIX Collaboration), Formation of dense partonic matter in relativistic nucleus-nucleus collisions at RHIC: Experimental evaluation by the PHENIX collaboration, Nucl. Phys. A **757**, 184 (2005).

[6] I. Arsene *et al.* (BRAHMS Collaboration), Quark gluon plasma and color glass condensate at RHIC? The perspective from the BRAHMS experiment, Nucl. Phys. A **757**, 1 (2005).

[7] B. B. Back *et al.* (PHOBOS Collaboration), The PHOBOS perspective on discoveries at RHIC, Nucl. Phys. A **757**, 28 (2005).

[8] K. Aamodt *et al.* (ALICE Collaboration), Elliptic Flow of Charged Particles in Pb-Pb Collisions at 2.76 TeV, Phys. Rev. Lett. **105**, 252302 (2010).

[9] K. Aamodt *et al.* (ALICE Collaboration), Higher Harmonic Anisotropic Flow Measurements of Charged Particles in Pb-Pb Collisions at $\sqrt{s_{NN}} = 2.76$ TeV, Phys. Rev. Lett. **107**, 032301 (2011).

[10] B. B. Abelev *et al.* (ALICE Collaboration), Elliptic flow of identified hadrons in Pb-Pb collisions at $\sqrt{s_{NN}} = 2.76$ TeV, J. High Energy Phys. 06 (2015) 190.

[11] J. Adam *et al.* (ALICE Collaboration), Anisotropic Flow of Charged Particles in Pb-Pb Collisions at $\sqrt{s_{NN}} = 5.02$ TeV, Phys. Rev. Lett. **116**, 132302 (2016).

[12] G. Aad *et al.* (ATLAS Collaboration), Measurement of the pseudorapidity and transverse momentum dependence of the elliptic flow of charged particles in lead-lead collisions at $\sqrt{s_{NN}} = 2.76$ TeV with the ATLAS detector, Phys. Lett. B **707**, 330 (2012).

[13] G. Aad *et al.* (ATLAS Collaboration), Measurement of the azimuthal anisotropy for charged particle production in $\sqrt{s_{NN}} =$ 2.76 TeV lead-lead collisions with the ATLAS detector, Phys. Rev. C **86**, 014907 (2012).

[14] G. Aad *et al.* (ATLAS Collaboration), Measurement of the distributions of event-by-event flow harmonics in lead-lead collisions at $\sqrt{s_{NN}} = 2.76$ TeV with the ATLAS detector at the LHC, J. High Energy Phys. 11 (2013) 183.

[15] G. Aad *et al.* (ATLAS Collaboration), Measurement of the centrality and pseudorapidity dependence of the integrated elliptic flow in lead-lead collisions at $\sqrt{s_{NN}} = 2.76$ TeV with the ATLAS detector, Eur. Phys. J. C **74**, 2982 (2014).

[16] S. Chatrchyan *et al.* (CMS Collaboration), Centrality dependence of dihadron correlations and azimuthal anisotropy harmonics in PbPb collisions at $\sqrt{s_{NN}} = 2.76$ TeV, Eur. Phys. J. C **72**, 2012 (2012).

[17] S. Chatrchyan *et al.* (CMS Collaboration), Measurement of the elliptic anisotropy of charged particles produced in PbPb collisions at $\sqrt{s_{NN}} = 2.76$ TeV, Phys. Rev. C **87**, 014902 (2013).

[18] S. Chatrchyan *et al.* (CMS Collaboration), Azimuthal Anisotropy of Charged Particles at High Transverse Momenta in PbPb Collisions at $\sqrt{s_{NN}} = 2.76$ TeV, Phys. Rev. Lett. **109**, 022301 (2012).

[19] P. Romatschke and U. Romatschke, Viscosity Information from Relativistic Nuclear Collisions: How Perfect is the Fluid Observed at RHIC? Phys. Rev. Lett. **99**, 172301 (2007).

[20] C. Shen, U. Heinz, P. Huovinen, and H. Song, Radial and elliptic flow in Pb+Pb collisions at the Large Hadron Collider from viscous hydrodynamic, Phys. Rev. C **84**, 044903 (2011).

[21] B. Schenke, S. Jeon, and C. Gale, Elliptic and triangular flows in 3+1D viscous hydrodynamics with fluctuating initial conditions, J. Phys. **G38**, 124169 (2011).

[22] P. Bozek and I. Wyskiel-Piekarska, Particle spectra in Pb-Pb collisions at $\sqrt{s_{NN}} = 2.76$ TeV, Phys. Rev. C **85**, 064915 (2012).

[23] C. Gale, S. Jeon, B. Schenke, P. Tribedy, and R. Venugopalan, Event-by-event Anisotropic Flow in Heavy-Ion Collisions from Combined Yang-Mills and Viscous Fluid Dynamics, Phys. Rev. Lett. **110**, 012302 (2013).

[24] T. Hirano, P. Huovinen, and Y. Nara, Elliptic flow in Pb+Pb collisions at $\sqrt{s_{NN}} = 2.76$ TeV: Hybrid model assessment of the first data, Phys. Rev. C **84**, 011901 (2011).

[25] P. K. Kovtun, D. T. Son, and A. O. Starinets, Viscosity in Strongly Interacting Quantum Field Theories from Black Hole Physics, Phys. Rev. Lett. **94**, 111601 (2005).

[26] R. A. Lacey, N. N. Ajitanand, J. M. Alexander, P. Chung, W. G. Holzmann, M. Issah, A. Taranenko, P. Danielewicz, and H. Stocker, Has the QCD Critical Point been Signaled by Observations at RHIC? Phys. Rev. Lett. **98**, 092301 (2007).

[27] P. Danielewicz and M. Gyulassy, Dissipative phenomena in quark-gluon plasmas, Phys. Rev. D **31**, 53 (1985).

[28] L. P. Csernai, J. I. Kapusta, and L. D. McLerran, On the Strongly-Interacting low-Viscosity Matter Created in Relativistic Nuclear Collisions, Phys. Rev. Lett. **97**, 152303 (2006).

[29] J.-Y. Ollitrault, Anisotropy as a signature of transverse collective flow, Phys. Rev. D **46**, 229 (1992).

[30] S. Voloshin and Y. Zhang, Flow study in relativistic nuclear collisions by Fourier expansion of azimuthal particle distributions, Z. Phys. C **70**, 665 (1996).

[31] A. M. Poskanzer and S. A. Voloshin, Methods for analyzing anisotropic flow in relativistic nuclear collisions, Phys. Rev. C **58**, 1671 (1998).

[32] S. Floerchinger, U. A. Wiedemann, A. Beraudo, L. Del Zanna, G. Inghirami, and V. Rolando, How (non-)linear is the hydrodynamics of heavy ion collisions? Phys. Lett. B **735**, 305 (2014).

[33] M. Miller and R. Snellings, Eccentricity fluctuations and its possible effect on elliptic flow measurements, arXiv:nucl-ex/0312008 [nucl-ex].

[34] B. Alver *et al.* (PHOBOS Collaboration), System Size, Energy, Pseudorapidity, and Centrality Dependence of Elliptic Flow, Phys. Rev. Lett. **98**, 242302 (2007).

[35] B. Alver and G. Roland, Collision geometry fluctuations and triangular flow in heavy-ion collisions, Phys. Rev. C **81**, 054905 (2010); **82**, 039903(E) (2010).

[36] H. Niemi, G. S. Denicol, H. Holopainen, and P. Huovinen, Event-by-event distributions of azimuthal asymmetries in ultrarelativistic heavy-ion collisions, Phys. Rev. C **87**, 054901 (2013).

[37] G. Aad *et al.* (ATLAS Collaboration), Measurement of event-plane correlations in $\sqrt{s_{NN}} = 2.76$ TeV lead-lead collisions with the ATLAS detector, Phys. Rev. C **90**, 024905 (2014).

[38] B. H. Alver, C. Gombeaud, M. Luzum, and J.-Y. Ollitrault, Triangular flow in hydrodynamics and transport theory, Phys. Rev. C **82**, 034913 (2010).

[39] M. Luzum and J.-Y. Ollitrault, Extracting the shear viscosity of the quark-gluon plasma from flow in ultra-central heavy-ion collisions, Nucl. Phys. A **904**, 377c (2013).

[40] C. Shen, S. A. Bass, T. Hirano, P. Huovinen, Z. Qiu, H. Song, and U. Heinz, The QGP shear viscosity: Elusive goal or just around the corner? J. Phys. **G38**, 124045 (2011).

[41] P. Bozek, Flow and interferometry in 3+1 dimensional viscous hydrodynamics, Phys. Rev. C **85**, 034901 (2012).

[42] J.-B. Rose, J.-F. Paquet, G. S. Denicol, M. Luzum, B. Schenke, S. Jeon, and C. Gale, Extracting the bulk viscosity of the quark gluon plasma, Nucl. Phys. A **931**, 926 (2014).

[43] S. Ryu, J. F. Paquet, C. Shen, G. S. Denicol, B. Schenke, S. Jeon, and C. Gale, Importance of the Bulk Viscosity of QCD in Ultrarelativistic Heavy-Ion Collisions, Phys. Rev. Lett. **115**, 132301 (2015).

[44] D. Teaney and L. Yan, Triangularity and dipole asymmetry in heavy ion collisions, Phys. Rev. C **83**, 064904 (2011).

[45] H. Niemi, K. J. Eskola, and R. Paatelainen, Event-by-event fluctuations in a perturbative QCD + saturation + hydrodynamics model: Determining QCD matter shear viscosity in ultrarelativistic heavy-ion collisions, Phys. Rev. C **93**, 024907 (2016).

[46] Z. Qiu and U. W. Heinz, Event-by-event shape and flow fluctuations of relativistic heavy-ion collision fireballs, Phys. Rev. C **84**, 024911 (2011).

[47] S. S. Gubser and A. Yarom, Conformal hydrodynamics in Minkowski and de Sitter spacetimes, Nucl. Phys. B **846**, 469 (2011).

[48] Y. Hatta, J. Noronha, G. Torrieri, and B.-W. Xiao, Flow harmonics within an analytically solvable viscous hydrodynamic model, Phys. Rev. D **90**, 074026 (2014).

[49] L. V. Bravina, B. H. Brusheim Johansson, G. K. Eyyubova, V. L. Korotkikh, I. P. Lokhtin, L. V. Malinina, S. V. Petrushanko, A. M. Snigirev, and E. E. Zabrodin, Higher harmonics of azimuthal anisotropy in relativistic heavy ion collisions in HYDJET++ model, Eur. Phys. J. C **74**, 2807 (2014).

[50] L. V. Bravina, B. H. Brusheim Johansson, G. K. Eyyubova, V. L. Korotkikh, I. P. Lokhtin, L. V. Malinina, S. V. Petrushanko, A. M. Snigirev, and E. E. Zabrodin, Hexagonal flow v6 as a superposition of elliptic v2 and triangular v3 flows, Phys. Rev. C **89**, 024909 (2014).

[51] F. G. Gardim, F. Grassi, M. Luzum, and J.-Y. Ollitrault, Mapping the hydrodynamic response to the initial geometry in heavy-ion collisions, Phys. Rev. C **85**, 024908 (2012).

[52] D. Teaney and L. Yan, Non linearities in the harmonic spectrum of heavy ion collisions with ideal and viscous hydrodynamics, Phys. Rev. C **86**, 044908 (2012).

[53] S. Acharya *et al.* (ALICE Collaboration), Linear and non-linear flow modes in Pb-Pb collisions at $\sqrt{s_{NN}} = 2.76$ TeV, Phys. Lett. B **773**, 68 (2017).

[54] M. Luzum and J.-Y. Ollitrault, Constraining the viscous freeze-out distribution function with data obtained at the BNL Relativistic Heavy Ion Collider (RHIC), Phys. Rev. C **82**, 014906 (2010).

[55] K. Dusling, G. D. Moore, and D. Teaney, Radiative energy loss and v(2) spectra for viscous hydrodynamics, Phys. Rev. C **81**, 034907 (2010).

[56] D. Molnar and Z. Wolff, Self-consistent conversion of a viscous fluid to particles, Phys. Rev. C **95**, 024903 (2017).

[57] J. Adam *et al.* (ALICE Collaboration), Correlated event-by-event Fluctuations of Flow Harmonics in Pb-Pb Collisions at $\sqrt{s_{NN}} = 2.76$ TeV, Phys. Rev. Lett. **117**, 182301 (2016).

[58] X. Zhu, Y. Zhou, H. Xu, and H. Song, Correlations of flow harmonics in 2.76A TeV Pb-Pb collisions, Phys. Rev. C **95**, 044902 (2017).

[59] H. Niemi, G. S. Denicol, P. Huovinen, E. Molnar, and D. H. Rischke, Influence of the Shear Viscosity of the Quark-Gluon Plasma on Elliptic Flow in Ultrarelativistic Heavy-Ion Collisions, Phys. Rev. Lett. **106**, 212302 (2011).

[60] A. Bilandzic, C. H. Christensen, K. Gulbrandsen, A. Hansen, and Y. Zhou, Generic framework for anisotropic flow analyses with multiparticle azimuthal correlations, Phys. Rev. C **89**, 064904 (2014).

[61] G. Giacalone, L. Yan, J. Noronha-Hostler, and J.-Y. Ollitrault, Symmetric cumulants and event-plane correlations in Pb + Pb collisions, Phys. Rev. C **94**, 014906 (2016).

[62] Y. Zhou, K. Xiao, Z. Feng, F. Liu, and R. Snellings, Anisotropic distributions in a multiphase transport model, Phys. Rev. C **93**, 034909 (2016).

[63] J. Qian and U. Heinz, Hydrodynamic flow amplitude correlations in event-by-event fluctuating heavy-ion collisions, Phys. Rev. C **94**, 024910 (2016).

[64] F. G. Gardim, F. Grassi, M. Luzum, and J. Noronha-Hostler, Hydrodynamic predictions for mixed harmonic correlations in 200 GeV Au+Au collisions, Phys. Rev. C **95**, 034901 (2017).

[65] W. Ke, J. S. Moreland, J. E. Bernhard, and S. A. Bass, Constraints on rapidity-dependent initial conditions from charged particle pseudorapidity densities and two-particle correlations, Phys. Rev. C **96**, 044912 (2017).

[66] K. Aamodt *et al.* (ALICE Collaboration), The ALICE experiment at the CERN LHC, JINST **3**, S08002 (2008).

[67] P. Cortese *et al.* (ALICE Collaboration), ALICE: Physics performance report, volume I, J. Phys. G **30**, 1517 (2004).

[68] P. Cortese *et al.* (ALICE Collaboration), ALICE: Physics performance report, volume II, J. Phys. G **32**, 1295 (2006).

[69] K. Aamodt *et al.* (ALICE Collaboration), Centrality Dependence of the Charged-Particle Multiplicity Density at Mid-Rapidity in Pb-Pb Collisions at $\sqrt{s_{NN}} = 2.76$ TeV, Phys. Rev. Lett. **106**, 032301 (2011).

[70] X.-N. Wang and M. Gyulassy, HIJING: A Monte Carlo model for multiple jet production in pp, pA, and AA collisions, Phys. Rev. D **44**, 3501 (1991).

[71] R. Brun, F. Bruyant, F. Carminati, S. Giani, M. Maire, A. McPherson, G. Patrick, and L. Urban, GEANT Detector Description and Simulation Tool (CERN, Geneva, 1993), p. 430.

[72] E. Abbas *et al.* (ALICE Collaboration), Performance of the ALICE VZERO system, JINST **8**, P10016 (2013).

[73] G. Dellacasa *et al.* (ALICE Collaboration), ALICE technical design report of the inner tracking system (ITS), CERN-LHCC-99-12 (1999).

[74] S. A. Voloshin, A. M. Poskanzer, and R. Snellings, Collective phenomena in non-central nuclear collisions, arXiv:0809.2949 [nucl-ex].

[75] B. Abelev *et al.* (ALICE Collaboration), Anisotropic flow of charged hadrons, pions, and (anti-)protons measured at high transverse momentum in Pb-Pb collisions at $\sqrt{s_{NN}} = 2.76$ TeV, Phys. Lett. B **719**, 18 (2013).

[76] C. Shen, U. Heinz, P. Huovinen, and H. Song, Systematic parameter study of hadron spectra and elliptic flow from viscous hydrodynamic simulations of Au+Au collisions at $\sqrt{s_{NN}} = 200$ GeV, Phys. Rev. C **82**, 054904 (2010).

[77] C. Shen, Z. Qiu, H. Song, J. Bernhard, S. Bass, and U. Heinz, The iEBE-VISHNU code package for relativistic heavy-ion collisions, Comput. Phys. Commun. **199**, 61 (2016).

[78] Z.-W. Lin, C. M. Ko, B.-A. Li, B. Zhang, and S. Pal, A multiphase transport model for relativistic heavy ion collisions, Phys. Rev. C **72**, 064901 (2005).

[79] Z.-W. Lin, Evolution of transverse flow and effective temperatures in the parton phase from a multiphase transport model, Phys. Rev. C **90**, 014904 (2014).

[80] R. Paatelainen, K. J. Eskola, H. Holopainen, and K. Tuominen, Multiplicities and p_T spectra in ultrarelativistic heavy ion collisions from a next-to-leading order improved perturbative QCD + saturation + hydrodynamics model, Phys. Rev. C **87**, 044904 (2013).

[81] R. Paatelainen, K. J. Eskola, H. Niemi, and K. Tuominen, Fluid dynamics with saturated minijet initial conditions in ultrarelativistic heavy-ion collisions, Phys. Lett. B **731**, 126 (2014).

[82] Z. Qiu, C. Shen, and U. Heinz, Hydrodynamic elliptic and triangular flow in Pb-Pb collisions at $\sqrt{s} = 2.76$ ATeV, Phys. Lett. B **707**, 151 (2012).

[83] R. S. Bhalerao, A. Jaiswal, and S. Pal, Collective flow in event-by-event partonic transport plus hydrodynamics hybrid approach, Phys. Rev. C **92**, 014903 (2015).

[84] P. F. Kolb, J. Sollfrank, and U. W. Heinz, Anisotropic transverse flow and the quark hadron phase transition, Phys. Rev. C **62**, 054909 (2000).

[85] D. Kharzeev and M. Nardi, Hadron production in nuclear collisions at RHIC and high density QCD, Phys. Lett. B **507**, 121 (2001).

[86] M. L. Miller, K. Reygers, S. J. Sanders, and P. Steinberg, Glauber modeling in high energy nuclear collisions, Annu. Rev. Nucl. Part. Sci. **57**, 205 (2007).

[87] H. J. Drescher and Y. Nara, Effects of fluctuations on the initial eccentricity from the color glass condensate in heavy ion collisions, Phys. Rev. C **75**, 034905 (2007).

[88] T. Hirano and Y. Nara, Eccentricity fluctuation effects on elliptic flow in relativistic heavy ion collisions, Phys. Rev. C **79**, 064904 (2009).

[89] L. Pang, Q. Wang, and X.-N. Wang, Effects of initial flow velocity fluctuation in event-by-event (3+1)D hydrodynamics, Phys. Rev. C **86**, 024911 (2012).

[90] H.-j. Xu, Z. Li, and H. Song, High-order flow harmonics of identified hadrons in 2.76A TeV Pb + Pb collisions, Phys. Rev. C **93**, 064905 (2016).

[91] A. Kurkela and Y. Zhu, Isotropization and Hydrodynamization in Weakly Coupled Heavy-Ion Collisions, Phys. Rev. Lett. **115**, 182301 (2015).

[92] B. Zhang, C. M. Ko, B.-A. Li, and Z.-w. Lin, A multiphase transport model for nuclear collisions at RHIC, Phys. Rev. C **61**, 067901 (2000).

[93] Z.-w. Lin, S. Pal, C. M. Ko, B.-A. Li, and B. Zhang, Charged particle rapidity distributions at relativistic energies, Phys. Rev. C **64**, 011902 (2001).

[94] M. Gyulassy and X.-N. Wang, HIJING 1.0: A Monte Carlo program for parton and particle production in high-energy hadronic and nuclear collisions, Comput. Phys. Commun. **83**, 307 (1994).

[95] B. Andersson, G. Gustafson, and B. Nilsson-Almqvist, A model for low $p(t)$ hadronic reactions, with generalizations to hadron-nucleus and nucleus-nucleus collisions, Nucl. Phys. B **281**, 289 (1987).

[96] B. Nilsson-Almqvist and E. Stenlund, Interactions between hadrons and nuclei: The Lund Monte Carlo, Fritiof version 1.6, Comput. Phys. Commun. **43**, 387 (1987).

[97] B. Zhang, ZPC 1.0.1: A Parton cascade for ultrarelativistic heavy ion collisions, Comput. Phys. Commun. **109**, 193 (1998).

[98] B. Li, A. T. Sustich, B. Zhang, and C. M. Ko, Studies of superdense hadronic matter in a relativistic transport model, Int. J. Mod. Phys. E **10**, 267 (2001).
[99] Z.-w. Lin and C. M. Ko, Partonic effects on the elliptic flow at RHIC, Phys. Rev. C **65**, 034904 (2002).
[100] J. Adam *et al.* (ALICE Collaboration), Higher harmonic flow coefficients of identified hadrons in Pb-Pb collisions at $\sqrt{s_{NN}} =$ 2.76 TeV, J. High Energy Phys. 09 (2016) 164.
[101] R. S. Bhalerao, J.-Y. Ollitrault, and S. Pal, Characterizing flow fluctuations with moments, Phys. Lett. B **742**, 94 (2015).
[102] R. S. Bhalerao, J.-Y. Ollitrault, and S. Pal, Event-plane correlators, Phys. Rev. C **88**, 024909 (2013).
[103] D. Teaney and L. Yan, Event-plane correlations and hydrodynamic simulations of heavy ion collisions, Phys. Rev. C **90**, 024902 (2014).

S. Acharya,[137] J. Adam,[96] D. Adamová,[93] J. Adolfsson,[32] M. M. Aggarwal,[98] G. Aglieri Rinella,[33] M. Agnello,[29] N. Agrawal,[46] Z. Ahammed,[137] N. Ahmad,[15] S. U. Ahn,[78] S. Aiola,[141] A. Akindinov,[63] M. Al-Turany,[106] S. N. Alam,[137] J. L. B. Alba,[111] D. S. D. Albuquerque,[122] D. Aleksandrov,[89] B. Alessandro,[57] R. Alfaro Molina,[73] A. Alici,[11,25,52] A. Alkin,[3] J. Alme,[20] T. Alt,[69] L. Altenkamper,[20] I. Altsybeev,[136] C. Alves Garcia Prado,[121] C. Andrei,[86] D. Andreou,[33] H. A. Andrews,[110] A. Andronic,[106] V. Anguelov,[103] C. Anson,[96] T. Antičić,[107] F. Antinori,[55] P. Antonioli,[52] R. Anwar,[124] L. Aphecetche,[114] H. Appelshäuser,[69] S. Arcelli,[25] R. Arnaldi,[57] O. W. Arnold,[104,34] I. C. Arsene,[19] M. Arslandok,[103] B. Audurier,[114] A. Augustinus,[33] R. Averbeck,[106] M. D. Azmi,[15] A. Badalà,[54] Y. W. Baek,[59,77] S. Bagnasco,[57] R. Bailhache,[69] R. Bala,[100] A. Baldisseri,[74] M. Ball,[43] R. C. Baral,[66,87] A. M. Barbano,[24] R. Barbera,[26] F. Barile,[51,31] L. Barioglio,[24] G. G. Barnaföldi,[140] L. S. Barnby,[92] V. Barret,[131] P. Bartalini,[7] K. Barth,[33] E. Bartsch,[69] M. Basile,[25] N. Bastid,[131] S. Basu,[139] G. Batigne,[114] B. Batyunya,[76] P. C. Batzing,[19] I. G. Bearden,[90] H. Beck,[103] C. Bedda,[62] N. K. Behera,[59] I. Belikov,[133] F. Bellini,[25,33] H. Bello Martinez,[2] R. Bellwied,[124] L. G. E. Beltran,[120] V. Belyaev,[82] G. Bencedi,[140] S. Beole,[24] A. Bercuci,[86] Y. Berdnikov,[95] D. Berenyi,[140] R. A. Bertens,[127] D. Berzano,[33] L. Betev,[33] A. Bhasin,[100] I. R. Bhat,[100] A. K. Bhati,[98] B. Bhattacharjee,[42] J. Bhom,[118] A. Bianchi,[24] L. Bianchi,[124] N. Bianchi,[49] C. Bianchin,[139] J. Bielčík,[37] J. Bielčíková,[93] A. Bilandzic,[34,104] G. Biro,[140] R. Biswas,[4] S. Biswas,[4] J. T. Blair,[119] D. Blau,[89] C. Blume,[69] G. Boca,[134] F. Bock,[103,81,33] A. Bogdanov,[82] L. Boldizsár,[140] M. Bombara,[38] G. Bonomi,[135] M. Bonora,[33] J. Book,[69] H. Borel,[74] A. Borissov,[17,103] M. Borri,[126] E. Botta,[24] C. Bourjau,[90] L. Bratrud,[69] P. Braun-Munzinger,[106] M. Bregant,[121] T. A. Broker,[69] M. Broz,[37] E. J. Brucken,[44] E. Bruna,[57] G. E. Bruno,[33,31] D. Budnikov,[108] H. Buesching,[69] S. Bufalino,[29] P. Buhler,[113] P. Buncic,[33] O. Busch,[130] Z. Buthelezi,[75] J. B. Butt,[14] J. T. Buxton,[16] J. Cabala,[116] D. Caffarri,[33,91] H. Caines,[141] A. Caliva,[62,106] E. Calvo Villar,[111] P. Camerini,[23] A. A. Capon,[113] F. Carena,[33] W. Carena,[33] F. Carnesecchi,[25,11] J. Castillo Castellanos,[74] A. J. Castro,[127] E. A. R. Casula,[53] C. Ceballos Sanchez,[9] P. Cerello,[57] S. Chandra,[137] B. Chang,[125] S. Chapeland,[33] M. Chartier,[126] S. Chattopadhyay,[137] S. Chattopadhyay,[109] A. Chauvin,[34,104] C. Cheshkov,[132] B. Cheynis,[132] V. Chibante Barroso,[33] D. D. Chinellato,[122] S. Cho,[59] P. Chochula,[33] M. Chojnacki,[90] S. Choudhury,[137] T. Chowdhury,[131] P. Christakoglou,[91] C. H. Christensen,[90] P. Christiansen,[32] T. Chujo,[130] S. U. Chung,[17] C. Cicalo,[53] L. Cifarelli,[11,25] F. Cindolo,[52] J. Cleymans,[99] F. Colamaria,[31] D. Colella,[33,64,51] A. Collu,[81] M. Colocci,[25] M. Concas,[57,a] G. Conesa Balbastre,[80] Z. Conesa del Valle,[60] M. E. Connors,[141,b] J. G. Contreras,[37] T. M. Cormier,[94] Y. Corrales Morales,[57] I. Cortés Maldonado,[2] P. Cortese,[30] M. R. Cosentino,[123] F. Costa,[33] S. Costanza,[134] J. Crkovská,[60] P. Crochet,[131] E. Cuautle,[71] L. Cunqueiro,[70] T. Dahms,[34,104] A. Dainese,[55] M. C. Danisch,[103] A. Danu,[67] D. Das,[109] I. Das,[109] S. Das,[4] A. Dash,[87] S. Dash,[46] S. De,[47,121] A. De Caro,[28] G. de Cataldo,[51] C. de Conti,[121] J. de Cuveland,[40] A. De Falco,[22] D. De Gruttola,[28,11] N. De Marco,[57] S. De Pasquale,[28] R. D. De Souza,[122] H. F. Degenhardt,[121] A. Deisting,[106,103] A. Deloff,[85] C. Deplano,[91] P. Dhankher,[46] D. Di Bari,[31] A. Di Mauro,[33] P. Di Nezza,[49] B. Di Ruzza,[55] T. Dietel,[99] P. Dillenseger,[69] R. Divià,[33] Ø. Djuvsland,[20] A. Dobrin,[33] D. Domenicis Gimenez,[121] B. Dönigus,[69] O. Dordic,[19] L. V. R. Doremalen,[62] A. K. Dubey,[137] A. Dubla,[106] L. Ducroux,[132] A. K. Duggal,[98] M. Dukhishyam,[87] P. Dupieux,[131] R. J. Ehlers,[141] D. Elia,[51] E. Endress,[111] H. Engel,[68] E. Epple,[141] B. Erazmus,[114] F. Erhardt,[97] B. Espagnon,[60] S. Esumi,[130] G. Eulisse,[33] J. Eum,[17] D. Evans,[110] S. Evdokimov,[112] L. Fabbietti,[104,34] J. Faivre,[80] A. Fantoni,[49] M. Fasel,[94,81] L. Feldkamp,[70] A. Feliciello,[57] G. Feofilov,[136] A. Fernández Téllez,[2] A. Ferretti,[24] A. Festanti,[27,33] V. J. G. Feuillard,[74,131] J. Figiel,[118] M. A. S. Figueredo,[121] S. Filchagin,[108] D. Finogeev,[61] F. M. Fionda,[20,22] M. Floris,[33] S. Foertsch,[75] P. Foka,[106] S. Fokin,[89] E. Fragiacomo,[58] A. Francescon,[33] A. Francisco,[114] U. Frankenfeld,[106] G. G. Fronze,[24] U. Fuchs,[33] C. Furget,[80] A. Furs,[61] M. Fusco Girard,[28] J. J. Gaardhøje,[90] M. Gagliardi,[24] A. M. Gago,[111] K. Gajdosova,[90] M. Gallio,[24] C. D. Galvan,[120] P. Ganoti,[84] C. Garabatos,[106] E. Garcia-Solis,[12] K. Garg,[26] C. Gargiulo,[33] P. Gasik,[104,34] E. F. Gauger,[119] M. B. Gay Ducati,[72] M. Germain,[114] J. Ghosh,[109] P. Ghosh,[137] S. K. Ghosh,[4] P. Gianotti,[49] P. Giubellino,[33,106,57] P. Giubilato,[27] E. Gladysz-Dziadus,[118] P. Glässel,[103] D. M. Goméz Coral,[73] A. Gomez Ramirez,[68] A. S. Gonzalez,[33] P. González-Zamora,[2] S. Gorbunov,[40] L. Görlich,[118] S. Gotovac,[117] V. Grabski,[73] L. K. Graczykowski,[138] K. L. Graham,[110] L. Greiner,[81] A. Grelli,[62] C. Grigoras,[33] V. Grigoriev,[82] A. Grigoryan,[1] S. Grigoryan,[76] J. M. Gronefeld,[106] F. Grosa,[29] J. F. Grosse-Oetringhaus,[33] R. Grosso,[106] L. Gruber,[113] F. Guber,[61] R. Guernane,[80] B. Guerzoni,[25] K. Gulbrandsen,[90] T. Gunji,[129] A. Gupta,[100] R. Gupta,[100] I. B. Guzman,[2] R. Haake,[33] C. Hadjidakis,[60] H. Hamagaki,[83] G. Hamar,[140] J. C. Hamon,[133] M. R. Haque,[62] J. W. Harris,[141] A. Harton,[12] H. Hassan,[80] D. Hatzifotiadou,[11,52] S. Hayashi,[129] S. T. Heckel,[69] E. Hellbär,[69] H. Helstrup,[35] A. Herghelegiu,[86] E. G. Hernandez,[2] G. Herrera Corral,[10] F. Herrmann,[70] B. A. Hess,[102] K. F. Hetland,[35]

H. Hillemanns,[33] C. Hills,[126] B. Hippolyte,[133] J. Hladky,[65] B. Hohlweger,[104] D. Horak,[37] S. Hornung,[106] R. Hosokawa,[130,80] P. Hristov,[33] C. Hughes,[127] T. J. Humanic,[16] N. Hussain,[42] T. Hussain,[15] D. Hutter,[40] D. S. Hwang,[18] S. A. Iga Buitron,[71] R. Ilkaev,[108] M. Inaba,[130] M. Ippolitov,[82,89] M. Irfan,[15] M. S. Islam,[109] M. Ivanov,[106] V. Ivanov,[95] V. Izucheev,[112] B. Jacak,[81] N. Jacazio,[25] P. M. Jacobs,[81] M. B. Jadhav,[46] J. Jadlovsky,[116] S. Jaelani,[62] C. Jahnke,[34] M. J. Jakubowska,[138] M. A. Janik,[138] P. H. S. Y. Jayarathna,[124] C. Jena,[87] S. Jena,[124] M. Jercic,[97] R. T. Jimenez Bustamante,[106] P. G. Jones,[110] A. Jusko,[110] P. Kalinak,[64] A. Kalweit,[33] J. H. Kang,[142] V. Kaplin,[82] S. Kar,[137] A. Karasu Uysal,[79] O. Karavichev,[61] T. Karavicheva,[61] L. Karayan,[103,106] P. Karczmarczyk,[33] E. Karpechev,[61] U. Kebschull,[68] R. Keidel,[143] D. L. D. Keijdener,[62] M. Keil,[33] B. Ketzer,[43] Z. Khabanova,[91] P. Khan,[109] S. A. Khan,[137] A. Khanzadeev,[95] Y. Kharlov,[112] A. Khatun,[15] A. Khuntia,[47] M. M. Kielbowicz,[118] B. Kileng,[35] B. Kim,[130] D. Kim,[142] D. J. Kim,[125] H. Kim,[142] J. S. Kim,[41] J. Kim,[103] M. Kim,[59] M. Kim,[142] S. Kim,[18] T. Kim,[142] S. Kirsch,[40] I. Kisel,[40] S. Kiselev,[63] A. Kisiel,[138] G. Kiss,[140] J. L. Klay,[6] C. Klein,[69] J. Klein,[33] C. Klein-Bösing,[70] S. Klewin,[103] A. Kluge,[33] M. L. Knichel,[33,103] A. G. Knospe,[124] C. Kobdaj,[115] M. Kofarago,[140] M. K. Köhler,[103] T. Kollegger,[106] V. Kondratiev,[136] N. Kondratyeva,[82] E. Kondratyuk,[112] A. Konevskikh,[61] M. Konyushikhin,[139] M. Kopcik,[116] M. Kour,[100] C. Kouzinopoulos,[33] O. Kovalenko,[85] V. Kovalenko,[136] M. Kowalski,[118] G. Koyithatta Meethaleveedu,[46] I. Králik,[64] A. Kravčáková,[38] L. Kreis,[106] M. Krivda,[110,64] F. Krizek,[93] E. Kryshen,[95] M. Krzewicki,[40] A. M. Kubera,[16] V. Kučera,[93] C. Kuhn,[133] P. G. Kuijer,[91] A. Kumar,[100] J. Kumar,[46] L. Kumar,[98] S. Kumar,[46] S. Kundu,[87] P. Kurashvili,[85] A. Kurepin,[61] A. B. Kurepin,[61] A. Kuryakin,[108] S. Kushpil,[93] M. J. Kweon,[59] Y. Kwon,[142] S. L. La Pointe,[40] P. La Rocca,[26] C. Lagana Fernandes,[121] Y. S. Lai,[81] I. Lakomov,[33] R. Langoy,[39] K. Lapidus,[141] C. Lara,[68] A. Lardeux,[74,19] A. Lattuca,[24] E. Laudi,[33] R. Lavicka,[37] R. Lea,[23] L. Leardini,[103] S. Lee,[142] F. Lehas,[91] S. Lehner,[113] J. Lehrbach,[40] R. C. Lemmon,[92] V. Lenti,[51] E. Leogrande,[62] I. León Monzón,[120] P. Lévai,[140] X. Li,[13] J. Lien,[39] R. Lietava,[110] B. Lim,[17] S. Lindal,[19] V. Lindenstruth,[40] S. W. Lindsay,[126] C. Lippmann,[106] M. A. Lisa,[16] V. Litichevskyi,[44] W. J. Llope,[139] D. F. Lodato,[62] P. I. Loenne,[20] V. Loginov,[82] C. Loizides,[81] P. Loncar,[117] X. Lopez,[131] E. López Torres,[9] A. Lowe,[140] P. Luettig,[69] J. R. Luhder,[70] M. Lunardon,[27] G. Luparello,[58,23] M. Lupi,[33] T. H. Lutz,[141] A. Maevskaya,[61] M. Mager,[33] S. Mahajan,[100] S. M. Mahmood,[19] A. Maire,[133] R. D. Majka,[141] M. Malaev,[95] L. Malinina,[76,c] D. Mal'Kevich,[63] P. Malzacher,[106] A. Mamonov,[108] V. Manko,[89] F. Manso,[131] V. Manzari,[51] Y. Mao,[7] M. Marchisone,[75,128] J. Mareš,[65] G. V. Margagliotti,[23] A. Margotti,[52] J. Margutti,[62] A. Marín,[106] C. Markert,[119] M. Marquard,[69] N. A. Martin,[106] P. Martinengo,[33] J. A. L. Martinez,[68] M. I. Martínez,[2] G. Martínez García,[114] M. Martinez Pedreira,[33] S. Masciocchi,[106] M. Masera,[24] A. Masoni,[53] E. Masson,[114] A. Mastroserio,[51] A. M. Mathis,[104,34] P. F. T. Matuoka,[121] A. Matyja,[127] C. Mayer,[118] J. Mazer,[127] M. Mazzilli,[31] M. A. Mazzoni,[56] F. Meddi,[21] Y. Melikyan,[82] A. Menchaca-Rocha,[73] E. Meninno,[28] J. Mercado Pérez,[103] M. Meres,[36] S. Mhlanga,[99] Y. Miake,[130] M. M. Mieskolainen,[44] D. L. Mihaylov,[104] K. Mikhaylov,[63,76] J. Milosevic,[19] A. Mischke,[62] A. N. Mishra,[47] D. Miśkowiec,[106] J. Mitra,[137] C. M. Mitu,[67] N. Mohammadi,[62] B. Mohanty,[87] M. Mohisin Khan,[15,d] D. A. Moreira De Godoy,[70] L. A. P. Moreno,[2] S. Moretto,[27] A. Morreale,[114] A. Morsch,[33] V. Muccifora,[49] E. Mudnic,[117] D. Mühlheim,[70] S. Muhuri,[137] M. Mukherjee,[4] J. D. Mulligan,[141] M. G. Munhoz,[121] K. Münning,[43] R. H. Munzer,[69] H. Murakami,[129] S. Murray,[75] L. Musa,[33] J. Musinsky,[64] C. J. Myers,[124] J. W. Myrcha,[138] D. Nag,[4] B. Naik,[46] R. Nair,[85] B. K. Nandi,[46] R. Nania,[52,11] E. Nappi,[51] A. Narayan,[46] M. U. Naru,[14] H. Natal da Luz,[121] C. Nattrass,[127] S. R. Navarro,[2] K. Nayak,[87] R. Nayak,[46] T. K. Nayak,[137] S. Nazarenko,[108] A. Nedosekin,[63] R. A. Negrao De Oliveira,[33] L. Nellen,[71] S. V. Nesbo,[35] F. Ng,[124] M. Nicassio,[106] M. Niculescu,[67] J. Niedziela,[138,33] B. S. Nielsen,[90] S. Nikolaev,[89] S. Nikulin,[89] V. Nikulin,[95] F. Noferini,[11,52] P. Nomokonov,[76] G. Nooren,[62] J. C. C. Noris,[2] J. Norman,[126] A. Nyanin,[89] J. Nystrand,[20] H. Oeschler,[17,103,e] S. Oh,[141] A. Ohlson,[33,103] T. Okubo,[45] L. Olah,[140] J. Oleniacz,[138] A. C. Oliveira Da Silva,[121] M. H. Oliver,[141] J. Onderwaater,[106] C. Oppedisano,[57] R. Orava,[44] M. Oravec,[116] A. Ortiz Velasquez,[71] A. Oskarsson,[32] J. Otwinowski,[118] K. Oyama,[83] Y. Pachmayer,[103] V. Pacik,[90] D. Pagano,[135] P. Pagano,[28] G. Paić,[71] P. Palni,[7] J. Pan,[139] A. K. Pandey,[46] S. Panebianco,[74] V. Papikyan,[1] G. S. Pappalardo,[54] P. Pareek,[47] J. Park,[59] S. Parmar,[98] A. Passfeld,[70] S. P. Pathak,[124] R. N. Patra,[137] B. Paul,[57] H. Pei,[7] T. Peitzmann,[62] X. Peng,[7] L. G. Pereira,[72] H. Pereira Da Costa,[74] D. Peresunko,[89,82] E. Perez Lezama,[69] V. Peskov,[69] Y. Pestov,[5] V. Petráček,[37] V. Petrov,[112] M. Petrovici,[86] C. Petta,[26] R. P. Pezzi,[72] S. Piano,[58] M. Pikna,[36] P. Pillot,[114] L. O. D. L. Pimentel,[90] O. Pinazza,[52,33] L. Pinsky,[124] D. B. Piyarathna,[124] M. Płoskoń,[81] M. Planinic,[97] F. Pliquett,[69] J. Pluta,[138] S. Pochybova,[140] P. L. M. Podesta-Lerma,[120] M. G. Poghosyan,[94] B. Polichtchouk,[112] N. Poljak,[97] W. Poonsawat,[115] A. Pop,[86] H. Poppenborg,[70] S. Porteboeuf-Houssais,[131] V. Pozdniakov,[76] S. K. Prasad,[4] R. Preghenella,[52] F. Prino,[57] C. A. Pruneau,[139] I. Pshenichnov,[61] M. Puccio,[24] G. Puddu,[22] P. Pujahari,[139] V. Punin,[108] J. Putschke,[139] S. Raha,[4] S. Rajput,[100] J. Rak,[125] A. Rakotozafindrabe,[74] L. Ramello,[30] F. Rami,[133] D. B. Rana,[124] R. Raniwala,[101] S. Raniwala,[101] S. S. Räsänen,[44] B. T. Rascanu,[69] D. Rathee,[98] V. Ratza,[43] I. Ravasenga,[29] K. F. Read,[127,94] K. Redlich,[85,f] A. Rehman,[20] P. Reichelt,[69] F. Reidt,[33] X. Ren,[7] R. Renfordt,[69] A. R. Reolon,[49] A. Reshetin,[61] K. Reygers,[103] V. Riabov,[95] R. A. Ricci,[50] T. Richert,[32] M. Richter,[19] P. Riedler,[33] W. Riegler,[33] F. Riggi,[26] C. Ristea,[67] M. Rodríguez Cahuantzi,[2] K. Røed,[19] E. Rogochaya,[76] D. Rohr,[33,40] D. Röhrich,[20] P. S. Rokita,[138] F. Ronchetti,[49] E. D. Rosas,[71] P. Rosnet,[131] A. Rossi,[27,55] A. Rotondi,[134] F. Roukoutakis,[84] A. Roy,[47] C. Roy,[133] P. Roy,[109] O. V. Rueda,[71] R. Rui,[23] B. Rumyantsev,[76] A. Rustamov,[88] E. Ryabinkin,[89] Y. Ryabov,[95] A. Rybicki,[118] S. Saarinen,[44] S. Sadhu,[137] S. Sadovsky,[112] K. Šafařík,[33] S. K. Saha,[137] B. Sahlmuller,[69] B. Sahoo,[46] P. Sahoo,[47] R. Sahoo,[47] S. Sahoo,[66] P. K. Sahu,[66] J. Saini,[137] S. Sakai,[130] M. A. Saleh,[139] J. Salzwedel,[16] S. Sambyal,[100] V. Samsonov,[95,82] A. Sandoval,[73] D. Sarkar,[137] N. Sarkar,[137] P. Sarma,[42] M. H. P. Sas,[62] E. Scapparone,[52] F. Scarlassara,[27] B. Schaefer,[94] R. P. Scharenberg,[105] H. S. Scheid,[69] C. Schiaua,[86] R. Schicker,[103] C. Schmidt,[106]

H. R. Schmidt,[102] M. O. Schmidt,[103] M. Schmidt,[102] N. V. Schmidt,[94,69] J. Schukraft,[33] Y. Schutz,[33,133] K. Schwarz,[106] K. Schweda,[106] G. Scioli,[25] E. Scomparin,[57] M. Šefčík,[38] J. E. Seger,[96] Y. Sekiguchi,[129] D. Sekihata,[45] I. Selyuzhenkov,[106,82] K. Senosi,[75] S. Senyukov,[3,133,33] E. Serradilla,[73] P. Sett,[46] A. Sevcenco,[67] A. Shabanov,[61] A. Shabetai,[114] R. Shahoyan,[33] W. Shaikh,[109] A. Shangaraev,[112] A. Sharma,[98] A. Sharma,[100] M. Sharma,[100] M. Sharma,[100] N. Sharma,[98,127] A. I. Sheikh,[137] K. Shigaki,[45] Q. Shou,[7] K. Shtejer,[9,24] Y. Sibiriak,[89] S. Siddhanta,[53] K. M. Sielewicz,[33] T. Siemiarczuk,[85] S. Silaeva,[89] D. Silvermyr,[32] C. Silvestre,[80] G. Simatovic,[97] G. Simonetti,[33] R. Singaraju,[137] R. Singh,[87] V. Singhal,[137] T. Sinha,[109] B. Sitar,[36] M. Sitta,[30] T. B. Skaali,[19] M. Slupecki,[125] N. Smirnov,[141] R. J. M. Snellings,[62] T. W. Snellman,[125] J. Song,[17] M. Song,[142] F. Soramel,[27] S. Sorensen,[127] F. Sozzi,[106] E. Spiriti,[49] I. Sputowska,[118] B. K. Srivastava,[105] J. Stachel,[103] I. Stan,[67] P. Stankus,[94] E. Stenlund,[32] D. Stocco,[114] M. M. Storetvedt,[35] P. Strmen,[36] A. A. P. Suaide,[121] T. Sugitate,[45] C. Suire,[60] M. Suleymanov,[14] M. Suljic,[23] R. Sultanov,[63] M. Šumbera,[93] S. Sumowidagdo,[48] K. Suzuki,[113] S. Swain,[66] A. Szabo,[36] I. Szarka,[36] U. Tabassam,[14] J. Takahashi,[122] G. J. Tambave,[20] N. Tanaka,[130] M. Tarhini,[60] M. Tariq,[15] M. G. Tarzila,[86] A. Tauro,[33] G. Tejeda Muñoz,[2] A. Telesca,[33] K. Terasaki,[129] C. Terrevoli,[27] B. Teyssier,[132] D. Thakur,[47] S. Thakur,[137] D. Thomas,[119] F. Thoresen,[90] R. Tieulent,[132] A. Tikhonov,[61] A. R. Timmins,[124] A. Toia,[69] S. R. Torres,[120] S. Tripathy,[47] S. Trogolo,[24] G. Trombetta,[31] L. Tropp,[38] V. Trubnikov,[3] W. H. Trzaska,[125] B. A. Trzeciak,[62] T. Tsuji,[129] A. Tumkin,[108] R. Turrisi,[55] T. S. Tveter,[19] K. Ullaland,[20] E. N. Umaka,[124] A. Uras,[132] G. L. Usai,[22] A. Utrobicic,[97] M. Vala,[116,64] J. Van Der Maarel,[62] J. W. Van Hoorne,[33] M. van Leeuwen,[62] T. Vanat,[93] P. Vande Vyvre,[33] D. Varga,[140] A. Vargas,[2] M. Vargyas,[125] R. Varma,[46] M. Vasileiou,[84] A. Vasiliev,[89] A. Vauthier,[80] O. Vázquez Doce,[104,34] V. Vechernin,[136] A. M. Veen,[62] A. Velure,[20] E. Vercellin,[24] S. Vergara Limón,[2] R. Vernet,[8] R. Vértesi,[140] L. Vickovic,[117] S. Vigolo,[62] J. Viinikainen,[125] Z. Vilakazi,[128] O. Villalobos Baillie,[110] A. Villatoro Tello,[2] A. Vinogradov,[89] L. Vinogradov,[136] T. Virgili,[28] V. Vislavicius,[32] A. Vodopyanov,[76] M. A. Völkl,[103,102] K. Voloshin,[63] S. A. Voloshin,[139] G. Volpe,[31] B. von Haller,[33] I. Vorobyev,[104,34] D. Voscek,[116] D. Vranic,[33,106] J. Vrláková,[38] B. Wagner,[20] H. Wang,[62] M. Wang,[7] D. Watanabe,[130] Y. Watanabe,[129,130] M. Weber,[113] S. G. Weber,[106] D. F. Weiser,[103] S. C. Wenzel,[33] J. P. Wessels,[70] U. Westerhoff,[70] A. M. Whitehead,[99] J. Wiechula,[69] J. Wikne,[19] G. Wilk,[85] J. Wilkinson,[103,52] G. A. Willems,[70] M. C. S. Williams,[52] E. Willsher,[110] B. Windelband,[103] W. E. Witt,[127] S. Yalcin,[79] K. Yamakawa,[45] P. Yang,[7] S. Yano,[45] Z. Yin,[7] H. Yokoyama,[130,80] I.-K. Yoo,[17] J. H. Yoon,[59] V. Yurchenko,[3] V. Zaccolo,[57] A. Zaman,[14] C. Zampolli,[33] H. J. C. Zanoli,[121] N. Zardoshti,[110] A. Zarochentsev,[136] P. Závada,[65] N. Zaviyalov,[108] H. Zbroszczyk,[138] M. Zhalov,[95] H. Zhang,[20,7] X. Zhang,[7] Y. Zhang,[7] C. Zhang,[62] Z. Zhang,[7,131] C. Zhao,[19] N. Zhigareva,[63] D. Zhou,[7] Y. Zhou,[90] Z. Zhou,[20] H. Zhu,[20] J. Zhu,[7] A. Zichichi,[25,11] A. Zimmermann,[103] M. B. Zimmermann,[33] G. Zinovjev,[3] J. Zmeskal,[113] and S. Zou[7]

(ALICE Collaboration)

[1]*A.I. Alikhanyan National Science Laboratory (Yerevan Physics Institute) Foundation, Yerevan, Armenia*
[2]*Benemérita Universidad Autónoma de Puebla, Puebla, Mexico*
[3]*Bogolyubov Institute for Theoretical Physics, Kiev, Ukraine*
[4]*Bose Institute, Department of Physics and Centre for Astroparticle Physics and Space Science (CAPSS), Kolkata, India*
[5]*Budker Institute for Nuclear Physics, Novosibirsk, Russia*
[6]*California Polytechnic State University, San Luis Obispo, California, USA*
[7]*Central China Normal University, Wuhan, China*
[8]*Centre de Calcul de l'IN2P3, Villeurbanne, Lyon, France*
[9]*Centro de Aplicaciones Tecnológicas y Desarrollo Nuclear (CEADEN), Havana, Cuba*
[10]*Centro de Investigación y de Estudios Avanzados (CINVESTAV), Mexico City and Mérida, Mexico*
[11]*Centro Fermi - Museo Storico della Fisica e Centro Studi e Ricerche "Enrico Fermi," Rome, Italy*
[12]*Chicago State University, Chicago, Illinois, USA*
[13]*China Institute of Atomic Energy, Beijing, China*
[14]*COMSATS Institute of Information Technology (CIIT), Islamabad, Pakistan*
[15]*Department of Physics, Aligarh Muslim University, Aligarh, India*
[16]*Department of Physics, Ohio State University, Columbus, Ohio, USA*
[17]*Department of Physics, Pusan National University, Pusan, Republic of Korea*
[18]*Department of Physics, Sejong University, Seoul, Republic of Korea*
[19]*Department of Physics, University of Oslo, Oslo, Norway*
[20]*Department of Physics and Technology, University of Bergen, Bergen, Norway*
[21]*Dipartimento di Fisica dell'Università 'La Sapienza' and Sezione INFN, Rome, Italy*
[22]*Dipartimento di Fisica dell'Università and Sezione INFN, Cagliari, Italy*
[23]*Dipartimento di Fisica dell'Università and Sezione INFN, Trieste, Italy*
[24]*Dipartimento di Fisica dell'Università and Sezione INFN, Turin, Italy*
[25]*Dipartimento di Fisica e Astronomia dell'Università and Sezione INFN, Bologna, Italy*
[26]*Dipartimento di Fisica e Astronomia dell'Università and Sezione INFN, Catania, Italy*
[27]*Dipartimento di Fisica e Astronomia dell'Università and Sezione INFN, Padova, Italy*

[28]*Dipartimento di Fisica 'E.R. Caianiello' dell'Università and Gruppo Collegato INFN, Salerno, Italy*
[29]*Dipartimento DISAT del Politecnico and Sezione INFN, Turin, Italy*
[30]*Dipartimento di Scienze e Innovazione Tecnologica dell'Università del Piemonte Orientale and INFN Sezione di Torino, Alessandria, Italy*
[31]*Dipartimento Interateneo di Fisica 'M. Merlin' and Sezione INFN, Bari, Italy*
[32]*Division of Experimental High Energy Physics, University of Lund, Lund, Sweden*
[33]*European Organization for Nuclear Research (CERN), Geneva, Switzerland*
[34]*Excellence Cluster Universe, Technische Universität München, Munich, Germany*
[35]*Faculty of Engineering, Bergen University College, Bergen, Norway*
[36]*Faculty of Mathematics, Physics and Informatics, Comenius University, Bratislava, Slovakia*
[37]*Faculty of Nuclear Sciences and Physical Engineering, Czech Technical University in Prague, Prague, Czech Republic*
[38]*Faculty of Science, P.J. Šafárik University, Košice, Slovakia*
[39]*Faculty of Technology, Buskerud and Vestfold University College, Tonsberg, Norway*
[40]*Frankfurt Institute for Advanced Studies, Johann Wolfgang Goethe-Universität Frankfurt, Frankfurt, Germany*
[41]*Gangneung-Wonju National University, Gangneung, Republic of Korea*
[42]*Gauhati University, Department of Physics, Guwahati, India*
[43]*Helmholtz-Institut für Strahlen- und Kernphysik, Rheinische Friedrich-Wilhelms-Universität Bonn, Bonn, Germany*
[44]*Helsinki Institute of Physics (HIP), Helsinki, Finland*
[45]*Hiroshima University, Hiroshima, Japan*
[46]*Indian Institute of Technology Bombay (IIT), Mumbai, India*
[47]*Indian Institute of Technology Indore, Indore, India*
[48]*Indonesian Institute of Sciences, Jakarta, Indonesia*
[49]*INFN, Laboratori Nazionali di Frascati, Frascati, Italy*
[50]*INFN, Laboratori Nazionali di Legnaro, Legnaro, Italy*
[51]*INFN, Sezione di Bari, Bari, Italy*
[52]*INFN, Sezione di Bologna, Bologna, Italy*
[53]*INFN, Sezione di Cagliari, Cagliari, Italy*
[54]*INFN, Sezione di Catania, Catania, Italy*
[55]*INFN, Sezione di Padova, Padova, Italy*
[56]*INFN, Sezione di Roma, Rome, Italy*
[57]*INFN, Sezione di Torino, Turin, Italy*
[58]*INFN, Sezione di Trieste, Trieste, Italy*
[59]*Inha University, Incheon, Republic of Korea*
[60]*Institut de Physique Nucléaire d'Orsay (IPNO), Université Paris-Sud, CNRS-IN2P3, Orsay, France*
[61]*Institute for Nuclear Research, Academy of Sciences, Moscow, Russia*
[62]*Institute for Subatomic Physics of Utrecht University, Utrecht, Netherlands*
[63]*Institute for Theoretical and Experimental Physics, Moscow, Russia*
[64]*Institute of Experimental Physics, Slovak Academy of Sciences, Košice, Slovakia*
[65]*Institute of Physics, Academy of Sciences of the Czech Republic, Prague, Czech Republic*
[66]*Institute of Physics, Bhubaneswar, India*
[67]*Institute of Space Science (ISS), Bucharest, Romania*
[68]*Institut für Informatik, Johann Wolfgang Goethe-Universität Frankfurt, Frankfurt, Germany*
[69]*Institut für Kernphysik, Johann Wolfgang Goethe-Universität Frankfurt, Frankfurt, Germany*
[70]*Institut für Kernphysik, Westfälische Wilhelms-Universität Münster, Münster, Germany*
[71]*Instituto de Ciencias Nucleares, Universidad Nacional Autónoma de México, Mexico City, Mexico*
[72]*Instituto de Física, Universidade Federal do Rio Grande do Sul (UFRGS), Porto Alegre, Brazil*
[73]*Instituto de Física, Universidad Nacional Autónoma de México, Mexico City, Mexico*
[74]*IRFU, CEA, Université Paris-Saclay, Saclay, France*
[75]*iThemba LABS, National Research Foundation, Somerset West, South Africa*
[76]*Joint Institute for Nuclear Research (JINR), Dubna, Russia*
[77]*Konkuk University, Seoul, Republic of Korea*
[78]*Korea Institute of Science and Technology Information, Daejeon, Republic of Korea*
[79]*KTO Karatay University, Konya, Turkey*
[80]*Laboratoire de Physique Subatomique et de Cosmologie, Université Grenoble-Alpes, CNRS-IN2P3, Grenoble, France*
[81]*Lawrence Berkeley National Laboratory, Berkeley, California, USA*
[82]*Moscow Engineering Physics Institute, Moscow, Russia*
[83]*Nagasaki Institute of Applied Science, Nagasaki, Japan*

[84]*National and Kapodistrian University of Athens, Physics Department, Athens, Greece*
[85]*National Centre for Nuclear Studies, Warsaw, Poland*
[86]*National Institute for Physics and Nuclear Engineering, Bucharest, Romania*
[87]*National Institute of Science Education and Research, HBNI, Jatni, India*
[88]*National Nuclear Research Center, Baku, Azerbaijan*
[89]*National Research Centre Kurchatov Institute, Moscow, Russia*
[90]*Niels Bohr Institute, University of Copenhagen, Copenhagen, Denmark*
[91]*Nikhef, Nationaal instituut voor subatomaire fysica, Amsterdam, Netherlands*
[92]*Nuclear Physics Group, STFC Daresbury Laboratory, Daresbury, United Kingdom*
[93]*Nuclear Physics Institute, Academy of Sciences of the Czech Republic, Řež u Prahy, Czech Republic*
[94]*Oak Ridge National Laboratory, Oak Ridge, Tennessee, USA*
[95]*Petersburg Nuclear Physics Institute, Gatchina, Russia*
[96]*Physics Department, Creighton University, Omaha, Nebraska, USA*
[97]*Physics department, Faculty of science, University of Zagreb, Zagreb, Croatia*
[98]*Physics Department, Panjab University, Chandigarh, India*
[99]*Physics Department, University of Cape Town, Cape Town, South Africa*
[100]*Physics Department, University of Jammu, Jammu, India*
[101]*Physics Department, University of Rajasthan, Jaipur, India*
[102]*Physikalisches Institut, Eberhard Karls Universität Tübingen, Tübingen, Germany*
[103]*Physikalisches Institut, Ruprecht-Karls-Universität Heidelberg, Heidelberg, Germany*
[104]*Physik Department, Technische Universität München, Munich, Germany*
[105]*Purdue University, West Lafayette, Indiana, USA*
[106]*Research Division and ExtreMe Matter Institute EMMI, GSI Helmholtzzentrum für Schwerionenforschung GmbH, Darmstadt, Germany*
[107]*Rudjer Bošković Institute, Zagreb, Croatia*
[108]*Russian Federal Nuclear Center (VNIIEF), Sarov, Russia*
[109]*Saha Institute of Nuclear Physics, Kolkata, India*
[110]*School of Physics and Astronomy, University of Birmingham, Birmingham, United Kingdom*
[111]*Sección Física, Departamento de Ciencias, Pontificia Universidad Católica del Perú, Lima, Peru*
[112]*SSC IHEP of NRC Kurchatov Institute, Protvino, Russia*
[113]*Stefan Meyer Institut für Subatomare Physik (SMI), Vienna, Austria*
[114]*SUBATECH, IMT Atlantique, Université de Nantes, CNRS-IN2P3, Nantes, France*
[115]*Suranaree University of Technology, Nakhon Ratchasima, Thailand*
[116]*Technical University of Košice, Košice, Slovakia*
[117]*Technical University of Split FESB, Split, Croatia*
[118]*The Henryk Niewodniczanski Institute of Nuclear Physics, Polish Academy of Sciences, Cracow, Poland*
[119]*The University of Texas at Austin, Physics Department, Austin, Texas, USA*
[120]*Universidad Autónoma de Sinaloa, Culiacán, Mexico*
[121]*Universidade de São Paulo (USP), São Paulo, Brazil*
[122]*Universidade Estadual de Campinas (UNICAMP), Campinas, Brazil*
[123]*Universidade Federal do ABC, Santo Andre, Brazil*
[124]*University of Houston, Houston, Texas, USA*
[125]*University of Jyväskylä, Jyväskylä, Finland*
[126]*University of Liverpool, Liverpool, United Kingdom*
[127]*University of Tennessee, Knoxville, Tennessee, USA*
[128]*University of the Witwatersrand, Johannesburg, South Africa*
[129]*University of Tokyo, Tokyo, Japan*
[130]*University of Tsukuba, Tsukuba, Japan*
[131]*Université Clermont Auvergne, CNRS/IN2P3, LPC, Clermont-Ferrand, France*
[132]*Université de Lyon, Université Lyon 1, CNRS/IN2P3, IPN-Lyon, Villeurbanne, Lyon, France*
[133]*Université de Strasbourg, CNRS, IPHC UMR 7178, F-67000 Strasbourg, France, Strasbourg, France*
[134]*Università degli Studi di Pavia, Pavia, Italy*
[135]*Università di Brescia, Brescia, Italy*
[136]*V. Fock Institute for Physics, St. Petersburg State University, St. Petersburg, Russia*
[137]*Variable Energy Cyclotron Centre, Kolkata, India*
[138]*Warsaw University of Technology, Warsaw, Poland*
[139]*Wayne State University, Detroit, Michigan, USA*
[140]*Wigner Research Centre for Physics, Hungarian Academy of Sciences, Budapest, Hungary*
[141]*Yale University, New Haven, Connecticut, USA*

[142] *Yonsei University, Seoul, Republic of Korea*
[143] *Zentrum für Technologietransfer und Telekommunikation (ZTT), Fachhochschule Worms, Worms, Germany*

[a]Dipartimento DET del Politecnico di Torino, Turin, Italy.
[b]Georgia State University, Atlanta, Georgia, USA.
[c]M.V. Lomonosov Moscow State University, D.V. Skobeltsyn Institute of Nuclear, Physics, Moscow, Russia.
[d]Department of Applied Physics, Aligarh Muslim University, Aligarh, India.
[e]Deceased.
[f]Institute of Theoretical Physics, University of Wroclaw, Poland.